

A Novel Automobile Antenna for Vehicles Communication of IoT Systems in 5G Network

Wei Luo (✉ luowei1@cqupt.edu.cn)

Chongqing University of Posts and Telecommunications <https://orcid.org/0000-0002-6192-4536>

Wuquan Chen

Chongqing University of Posts and Telecommunications

Yulu Feng

Chongqing University of Posts and Telecommunications

Yuqi Yang

Chongqing University of Posts and Telecommunications

Research

Keywords: Automobile antenna, Internet of vehicles, Network performance

Posted Date: September 3rd, 2020

DOI: <https://doi.org/10.21203/rs.3.rs-26848/v2>

License: © ⓘ This work is licensed under a Creative Commons Attribution 4.0 International License.

[Read Full License](#)

Version of Record: A version of this preprint was published on October 29th, 2020. See the published version at <https://doi.org/10.1186/s13638-020-01838-7>.

A Novel Automobile Antenna for Vehicles Communication of IoT Systems in 5G Network

Wei Luo^{1*}, Wuquan Chen¹, Yulu Feng¹, Yuqi Yang²

*Correspondence: luowei1@cqupt.edu.cn, College of Electronic Engineering, Chongqing University of Posts and Telecommunications, Chongqing 400065, China, Full list of author information is available at the end of the article.

Abstract

The Internet of vehicles (IoV) is an important part of mobile communication system with the development of Internet of things (IoT). A novel multiband automobile antenna is proposed, which can cover all frequency bands for the long-term evolution (LTE), the 5th generation wireless systems (5G), the wireless local area network (WLAN) and the dedicated short-range communication (DSRC) (from 690 MHz to 944 MHz and from 1.46 GHz to 6 GHz). The antenna is designed based on the monopole antenna, and the impedance matching performance of the antenna is improved by loading the toothed capacitor and the impedance matching disc. The simulation results show that the automobile antenna achieves good impedance matching in the working bandwidth and obtains omnidirectional radiation pattern in the horizontal direction. The electric field distribution of the antenna placed on the vehicle roof is simulated to evaluate the network performance of the antenna system in the urban environment. The transmission coefficient of the transceiver system using the automobile antenna is also analyzed based on the electromagnetic simulation results and statistical model. The blind area of mobile communication system is effectively covered with the automobile antenna, which could be used to connect the LTE cell and the IoV system.

Keywords: Automobile antenna, Internet of vehicles, Network performance

1 Introduction

In order to meet the different needs of modern mobile communication, vehicles are loaded with

various functional antennas, which can be used in emergency call, entertainment, navigation and positioning [1]. The performance of automobile antenna is of great significance to improve the quality of service (QoS) in vehicle wireless communication system.

The long-term evolution (LTE) is suitable for automotive applications with the high data rate and scalability, since the peak data rate of the downlink stream and the uplink stream are 100 Mbit/s and 10 Mbit/s respectively [2]. Furthermore, the fifth generation mobile communication system (5G) incorporates the Internet of Things (IoT) system, lower round trip delays and a reduction in energy consumption [1]. IEEE has revised the 802.11 standard with 802.11p wireless access in DSRC for vehicle to vehicle (V2V) and vehicle to infrastructure (V2I) system [3][4]. There is an anticipated development prospect for the Internet of vehicles (IoV) system based on these requirements.

IoT is a global network system that enables a variety of physical, mechanical, electrical and electronic objects to connect and transmit data among billions of devices [5]. The V2V communication system could be established to improve road communication more effectively, in which the data from the vehicles as taken by numerous sensors would be uploaded to the database using IoT [6].

There are two implementable schemes for vehicle to everything (V2X): DSRC and LTE. DSRC refers to exchanging information between automobiles in a short distance through wireless technology. DSRC technology adopts the following equipment: a) on-board device (OBU) located inside the vehicle; b) road test unit (RSU) located on the side of the road; c) hand-held device carried by pedestrians [7]. The OBU installed in the vehicle communicates with the RSU installed on the roadside through microwave for the ETC systems of highway toll collection. 3GPP organization stipulates that vehicles can communicate with everything in the LTE technology [8]. The V2X

includes four types: V2V, V2I, vehicle to network (V2N) and vehicle to pedestrian (V2P). Fig. 1 shows the scenarios of V2X in the future IoT systems.

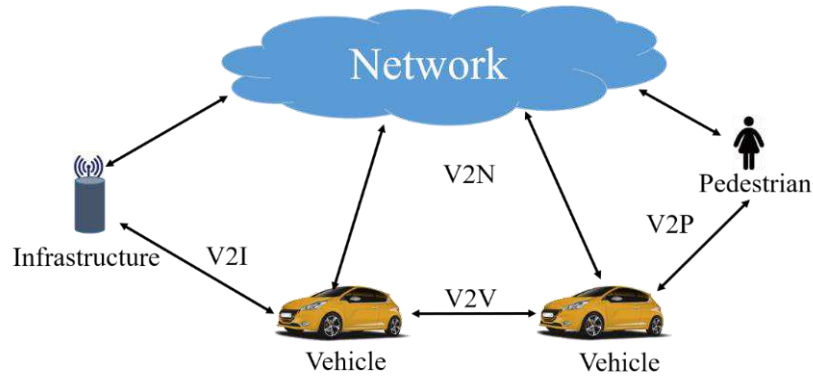


Fig. 1 Various V2X scenarios in IoT systems.

The vehicles will be combined with more communication devices to achieve more comprehensive and intelligent driving functions in the future traffic systems. An important challenge is how to integrate the antenna into a specific small volume model, such as the shark-fin shaped roof antenna. Meanwhile, how to realize a wide range of services in several frequency bands is also an important problem to solve. While multiple antennas of different frequency bands can be integrated into a fixed volume model, it is significant to reduce the coupling between the antennas and improve the radiation efficiency [9]. The literature [10] presents a new decoupling and matching network design for symmetric, single- and dual-band two-element antenna arrays. A multi-functional microstrip-fed ultra-wideband monopole antenna with two dual-mode resonators and shunt metallic strips has been presented, which two additional operational states are created [11]. A new planar microstrip-fed monopole ultra-wideband antenna with dual notched bands has been presented in the literature [12]. Due to the difficulty in improvement of the antenna isolation, the multiband antenna is widely researched to cover multiple frequency bands.

Various types of automobile antennas for the IoT systems have been investigated with different

methods based on the cost and efficiency of the antenna [13-16]. The broadband intelligent shark-fin antenna is designed for LTE, WLAN and DSRC communication systems, and applied in automobile communication [17]. The antenna integrates passive antenna radiator, active transceiver and software radio platform on a multilayer PCB. These complex systems enable the antenna to execute multiple communication systems at the same time. However, designing and machining the multiband antenna are relatively complex with high manufacturing cost.

In this paper, a novel multiband shark-fin automobile antenna is investigated, which can work in LTE, 5G, WLAN and DSRC bands (690 MHz to 944 MHz and 1.46 GHz to 6 GHz) for vehicles communication in IoT system. The paper is organized as followed. Section II illustrates the design and simulated results of the proposed automobile antenna. The network performance of the automobile antenna in V2X communication scenes is analyzed in Section III. Section IV analyzes the extended network coverage of the automobile antennas in the IoV systems. Section V concludes this paper finally.

2 Methods of Antenna design

2.1 Principle of monopole antenna

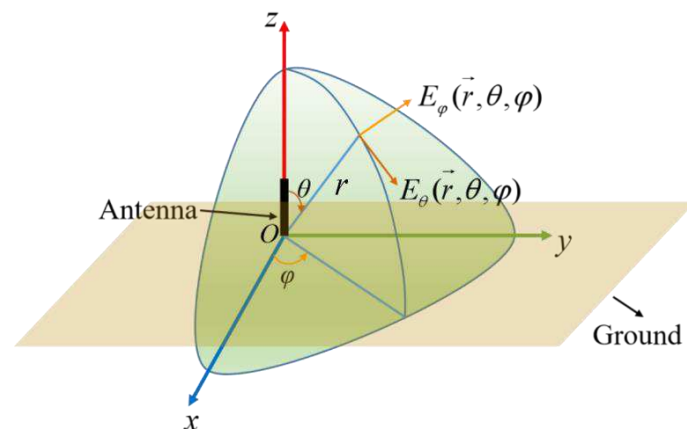


Fig. 2 Schematic diagram of simple antenna radiator.

An ideal monopole antenna is on the infinite ground, as shown in Fig. 2. The radiation pattern of the antenna can be calculated by the following equations.

$$E = \frac{60I_m}{r} \cdot \frac{\cos(\beta l \cos \theta) - \cos \beta l}{\sin \theta} \quad (1)$$

$$I_m = I_0 / \sin \beta l \quad (2)$$

I_m is antinode current and I_0 is input current, which are related to the input power of the antenna port. l is the effective length of the monopole antenna. β is the phase constant. The radiation pattern is a circle on the horizontal plane perpendicular to the antenna, which can provide omnidirectional radiation to meet the requirements of vehicle communication network coverage. The radiation resistance of monopole antenna is related to the effective length l .

$$R_{rm} \approx 160\pi^4 \left(\frac{l}{\lambda}\right)^4 \quad (3)$$

$$R_{ro} \approx 160\pi^2 \left(\frac{l}{\lambda}\right) \quad (4)$$

Eq. 3 is the radiation resistance of the wave belly current, and Eq. 4 is the radiation resistance of the input current. λ is operation wavelength. The radiation resistance of monopole antenna increases with the effective length of antenna. The antenna is fed by the coaxial line along the z-axis at the origin point as shown in Fig. 2. Eq. 5 is the Gaussian pulse signal feeding monopole along the coaxial line, where T_p is pulse period.

$$V(t) = -(t/T_p) \exp\left[0.5 - 0.5(t/T_p)^2\right] \quad (5)$$

The time domain gain of the antenna is defined as

$$G(\theta) = \frac{2\pi Z_c r^2}{\eta_0} \cdot \frac{\int_{-\infty}^{+\infty} |E(t, r, \theta)|^2 dt}{\int_{-\infty}^{+\infty} (|V_i(t)|^2 - |V_f(t)|^2) dt} \quad (6)$$

where V_i is the incident voltage in the coaxial line and V_f is the reflected voltage in the coaxial line. η_0 is the wave impedance in the free space. Z_c is the characteristic impedance of the coaxial

line.

The frequency domain gain of monopole antenna in a certain direction is

$$G_{\theta}(\omega) = \frac{2\pi Z_c r^2}{\eta_0} \cdot \frac{|E_{\theta}^r(\omega)|^2}{|V_i(\omega)|^2 - |V_r(\omega)|^2} \quad (7)$$

Eq. 6 and Eq. 7 show that the radiation ability of antenna to different frequency components is equivalent to each other in a sufficiently wide frequency band, which can achieve multiband working performance.

2.2 Multiband automobile antenna design

The novel automobile antenna for vehicles communication is designed to work in multiple frequency bands, covering all LTE, 5G, WLAN and DSRC bands. Three different structural antennas are discussed based on the electrical properties and structural features as shown in Fig. 3.

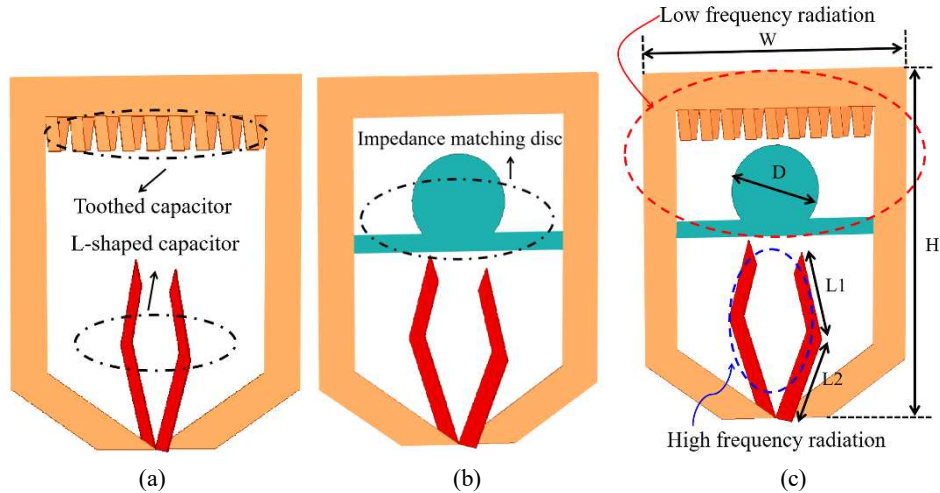


Fig. 3 Three kinds of rooftop antennas with different performance.

The antenna (a) has a toothed capacitor structure, and the antenna (b) has impedance matching disc. Both the toothed capacitor and the impedance matching disc can improve the impedance matching of the antenna by changing the current path on the antenna surface. The toothed capacitor loaded on the monopole reduces the overall height of the radiator, which is formed like a ridge structure. The two inductive vertical arms are connected to the feed point for the impedance

matching of the low frequency band (690 MHz - 944 MHz), and the impedance matching disc is used to improve impedance matching in the high frequency band (1.46 GHz - 6 GHz). Two L-shaped radiators are used as the high frequency radiators. Since the toothed capacitor and impedance matching disc have good effect on impedance matching, no additional matching network is needed in the design of the automobile antenna. The novel automobile antenna (c) is proposed based on the antenna (a) and antenna (b), and the specific parameters are shown in Table 1. The antenna is placed on a 250 mm × 250 mm ground. The impedance matching and radiation pattern of the antenna are affected by the size of the ground.

Table 1. Structure parameters of the antenna.

Structural parameters	W	H	L1	L2	D
Values [mm]	60	76	20	29	26.4

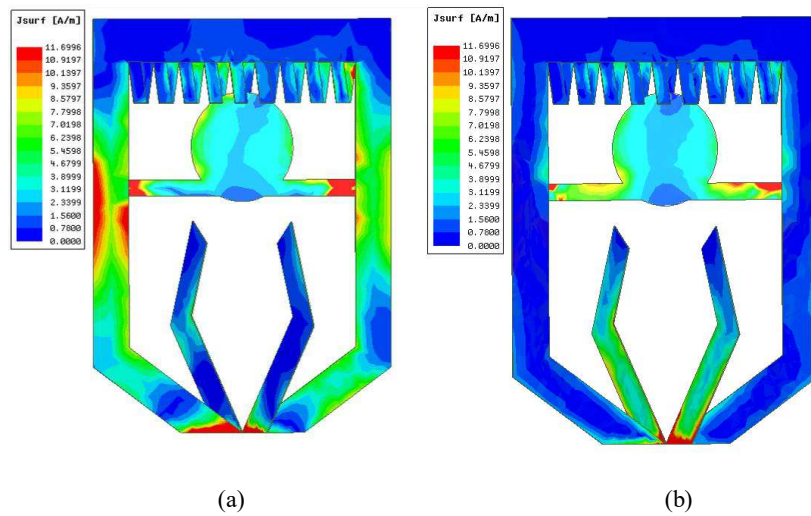


Fig. 4 The electrical current distributions at different frequencies.

The current distribution is shown in the Fig. 4 when the antenna is working at 900 MHz and 3 GHz. The loop monopole serves as the low frequency radiator of the antenna and two L-shaped monopoles serve as the high frequency radiator. The height of the low frequency radiator is 76 mm, which corresponds to an electrical size of roughly $\lambda/4$ at 900 MHz. Therefore, the low frequency radiator is the main radiation part when the antenna works in the low frequency band. However, the

height of the high frequency radiator is approximately 35 mm, which corresponds to an electrical size of roughly $\lambda/4$ at 3 GHz. Therefore, the high frequency radiator plays a leading role when the antenna works in a high frequency band. The antenna expands the impedance bandwidth of the antenna by loading the toothed capacitor and the impedance matching disc, which achieves wideband characteristics.

2.3 Results of antenna performance simulation

The frequency response characteristic curves of the input impedance are shown in the Fig. 5. The antenna (a) with a toothed capacitor structure has a good impedance matching at 2.5 GHz because the input impedance of the antenna (a) is close to 50 ohms. The S11 of the antenna (b) with impedance matching disc reaches -18 dB at 2.9 GHz due to its good impedance characteristics. Since the antenna (c) is loaded with a toothed capacitor and impedance matching disc, the impedance characteristic of the antenna (c) is improved to obtain a good impedance matching at 810 MHz and 2.9 GHz.

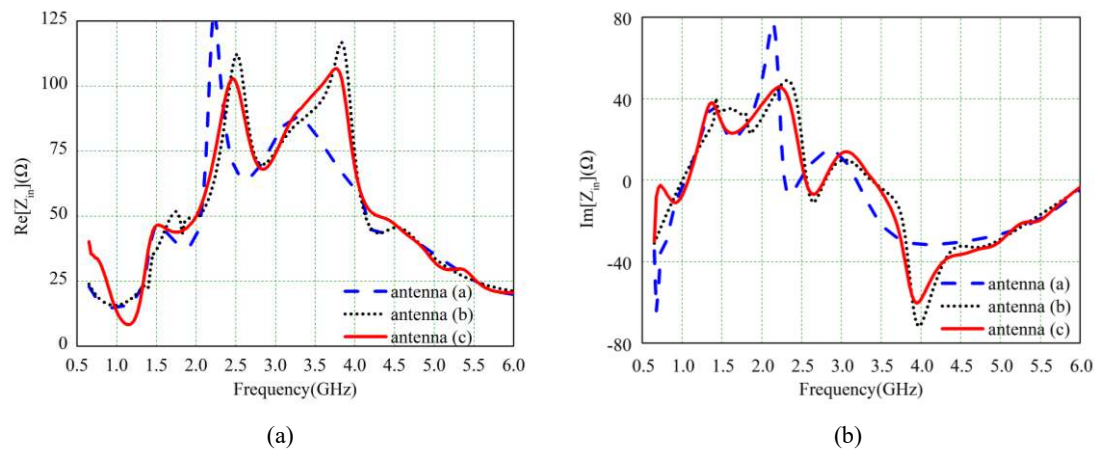


Fig. 5 Input impedance of the antennas.

Figure 6 shows the comparison of impedance matching for the three antenna designs. The S11 parameters of all the antenna designs are lower than -6 dB in the LTE, 5G and DSRC frequency bands, which is apparently sufficient for the transceivers of V2X systems. Since the antennas are

added with the impedance matching discs, the high frequency resonance points move to a higher frequency. It is found that the antenna (c) satisfies the requirements to impedance matching at the frequency regions from 690 MHz to 944 MHz and from 1.46 GHz to 6 GHz.

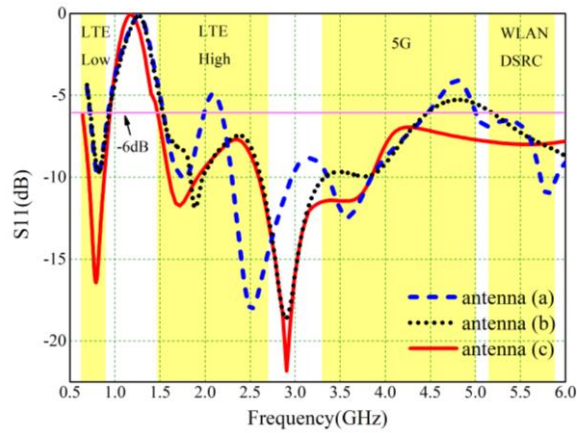


Fig. 6 S parameters of the rooftop antennas.

Since the antenna is designed for vehicle communication, the ground can be approximately described by an infinite perfect conducting plane. When the antenna is installed on the roof of the vehicle, the main beam direction (MBD) of the antenna is close to the horizontal direction. The omnidirectional radiation is satisfied for V2V communication.

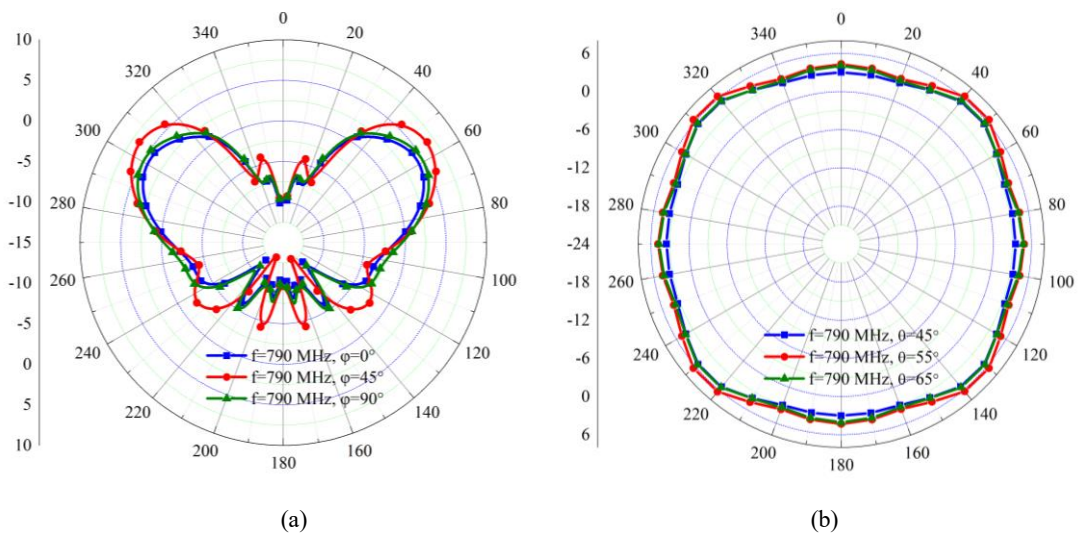


Fig. 7 The radiation pattern of antenna at 790 MHz.

Radiation patterns of the automobile antenna for LTE/5G communication at the several operation frequencies are shown from Fig. 7 to Fig. 11. The vertical radiation pattern of the antenna at 790

MHz is shown in Fig. 7a, in which the MBD of the antenna is directed towards an elevation angle of around 60° from zenith. Fig. 7b shows the horizontal radiation pattern of the MBD. The antenna achieves omnidirectional radiation at each elevation angle in the beam-width. The maximum gain of the antenna is 6.4 dBi and the deviation at all azimuth angles is just ± 1.8 dB.

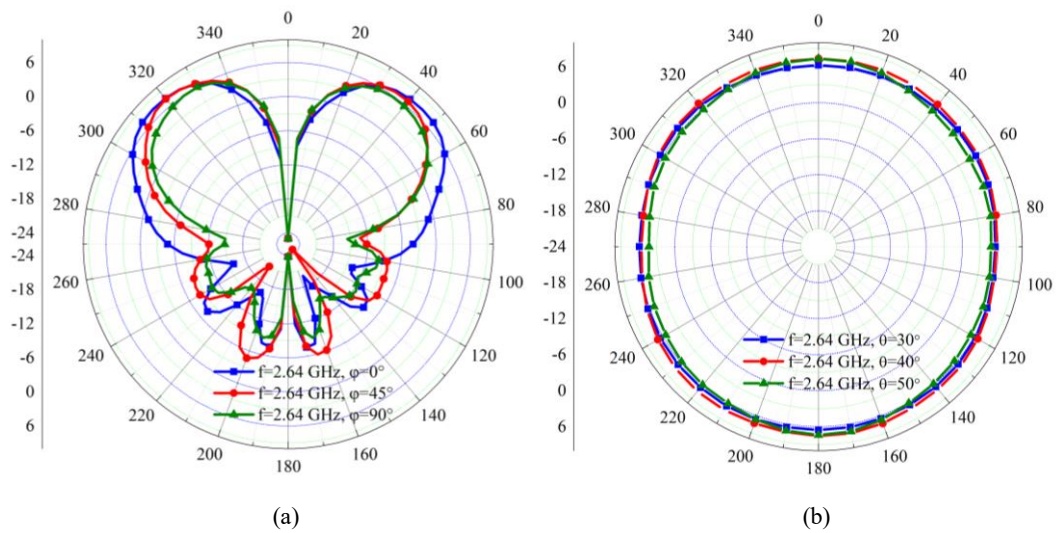


Fig. 8 The radiation pattern of antenna at 2.64 GHz.

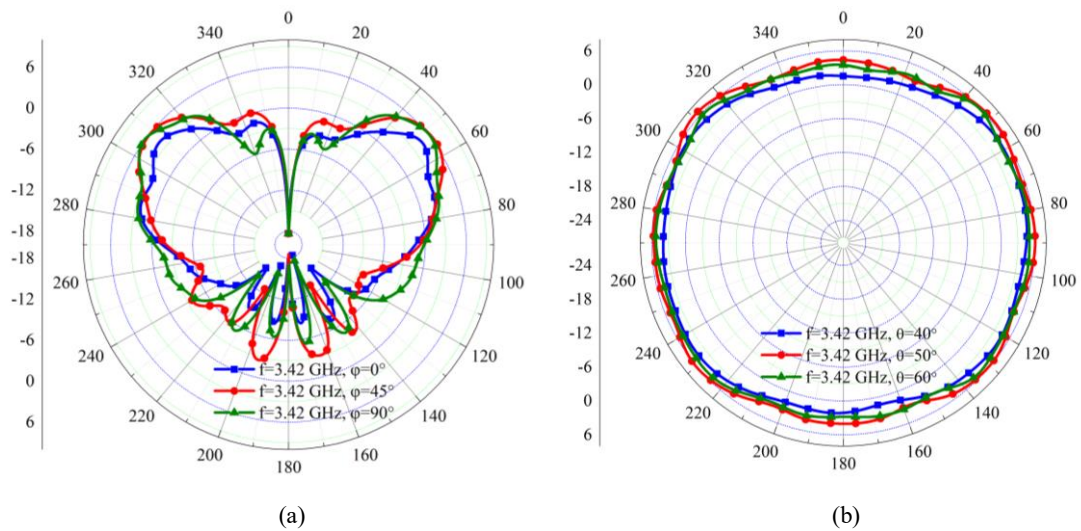


Fig. 9 The radiation pattern of antenna at 3.42 GHz.

Figure 8 shows the radiation patterns of the automobile antenna at 2.64 GHz. The MBD of the antenna is directed towards an elevation angle of around 40° from zenith. And the antenna still satisfies the characteristics of omnidirectional radiation at each elevation angle. The maximum gain of the antenna is 7.6 dBi and the deviation at all azimuth angles is just ± 1.5 dB.

Figure 9 shows the radiation patterns for the 5G system at 3.42 GHz, of which the MBD elevation angle is 55° from zenith. The maximum gain of the antenna is 6.9 dBi and the deviation at all azimuth angles is just ± 1.8 dB. As shown in Fig. 8a and Fig. 9a, the MBD of the antenna is no longer in the horizontal plane in the LTE band and the 5G band, but it is beneficial for the communication between the vehicles and the cellular base stations.

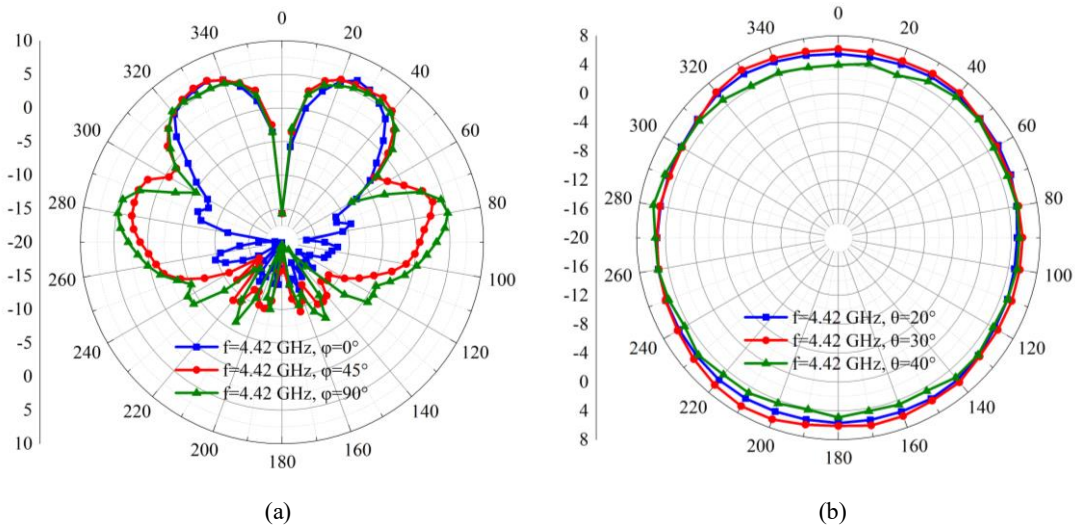


Fig. 10 The radiation pattern of antenna at 4.42 GHz.

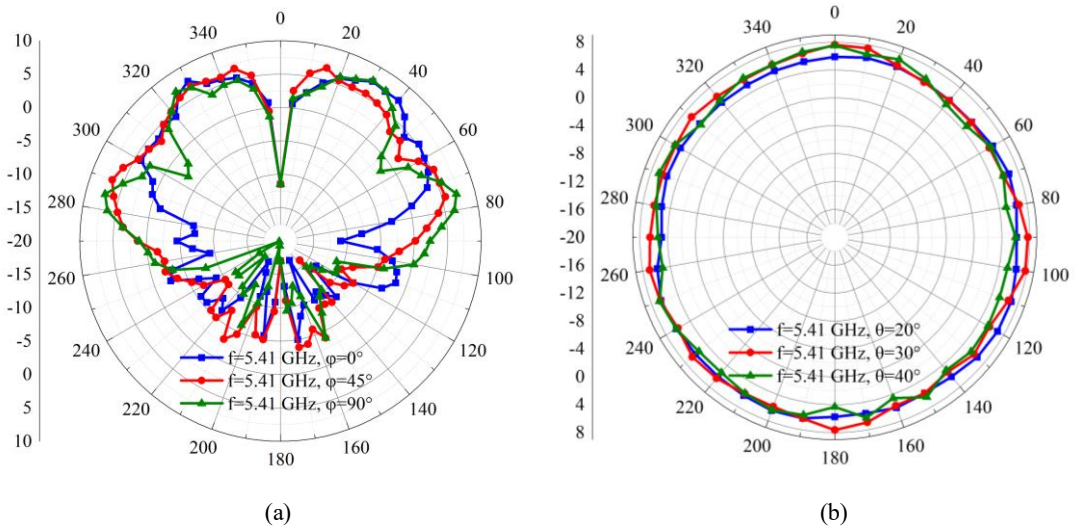


Fig. 11 The radiation pattern of antenna at 5.41 GHz.

Since the wavelength of electromagnetic wave radiated by the antenna is shorter when the antenna works at high frequency band, the electromagnetic wave is easily blocked by the roadside infrastructures. The higher gain of automobile antenna is required to cover communication network

effectively. The designed antenna has high directional gain, as shown from Fig. 7 to Fig. 11, which can effectively maintain vehicle communication.

3 Evaluation of antenna performance for V2X system

3.1 Path loss model for V2X system

According to the distribution characteristics of urban block scene in V2V communication, the conventional channel model is constructed to simulate the attenuation and interference of signals accurately, which is used to evaluate the feasibility of 5G vehicle network resource allocation algorithm [18]. The shadow fading follows normal distribution in V2V communication, and the definition of shadow fading is as followed

$$n_s(t) = \frac{1}{\sqrt{2\pi}\sigma} \exp\left(-\frac{(t-\mu)^2}{2\sigma^2}\right) \quad (8)$$

where μ is the expectation, and σ is the standard deviation. σ^2 is variance of the distribution.

The 5G NR-V2V communication operates in the Sub-6 GHz spectrum bands. The channel model of WINNER+B1 can be used in the urban block scene in Sub-6 GHz band [19]. It is assumed that the antenna height of the user terminal is much lower than the height of the surrounding buildings. The signal transmission condition includes the light of sight (LOS) and the not line of sight (NLOS) channels in the outdoor environment.

According to WINNER channel model, the path loss model in Sub-6 GHz band can be defined as

$$PL[\text{dB}] = A \log_{10}(d) + B + C \log_{10}(f_c/5.0) \quad (9)$$

where d is the distance between transmitter and receiver, and f_c is system frequency. A is the path loss index, and B is the intercept coefficient. C is the path loss frequency dependence coefficient.

The path loss model of LOS channel is

$$PL[\text{dB}] = \begin{cases} 22.7 \log_{10}(3) + 27.0 + 20.0 \log_{10}(f_c), & d \leq 3 \\ 22.7 \log_{10}(d) + 27.0 + 20.0 \log_{10}(f_c), & 3 < d \leq d_{BP} \\ 40.0 \log_{10}(d) + 7.56 - 17.3 \log_{10}(h'_{Tx}), & d > d_{BP} \\ -17.3 \log_{10}(h'_{Rx}) + 2.7 \log_{10}(f_c), & d > d_{BP} \end{cases} \quad (10)$$

where d is the distance between transmitter and receiver, f_c is system frequency. $d_{BP} = 4h'_{Tx}h'_{Rx}f_c/c$, $h'_{Tx} = h_{Tx} - 1$, $h'_{Rx} = h_{Rx} - 1$ and $c = 3 \times 10^8$ m/s. h_{Tx} and h_{Rx} are the antenna height of transmitter and the one of receiver respectively.

The path loss model of NLOS is defined as

$$PL = \min \{ PL(d_1, d_2), PL(d_2, d_1) \} \quad (11)$$

where d_1 is the vertical distance from the transmitter to the street center, d_2 is the vertical distance from the street center to the receiver. $PL(d_k, d_l)_{k \in \{1,2\}, l \in \{1,2\}}$ can be given as

$$PL(d_k, d_l) = PL_{LOS}(d_k) + 17.3 - 12.5\eta_j + 10\eta_j \log(d_j) + 3 \log_{10}(f_c) \quad (12)$$

$$\eta_j = \max(2.8 - 0.002d_k, 1.84). \quad (13)$$

where PL_{LOS} is the path loss of the LOS model.

The received signal strength indicator (RSSI) is given as Eq. 14, where P_{TRX} is the transmitted power of the TRX. $PL(\text{dB})$ is the path loss in the distance and $G_a(\theta, \varphi)$ is the antenna gain.

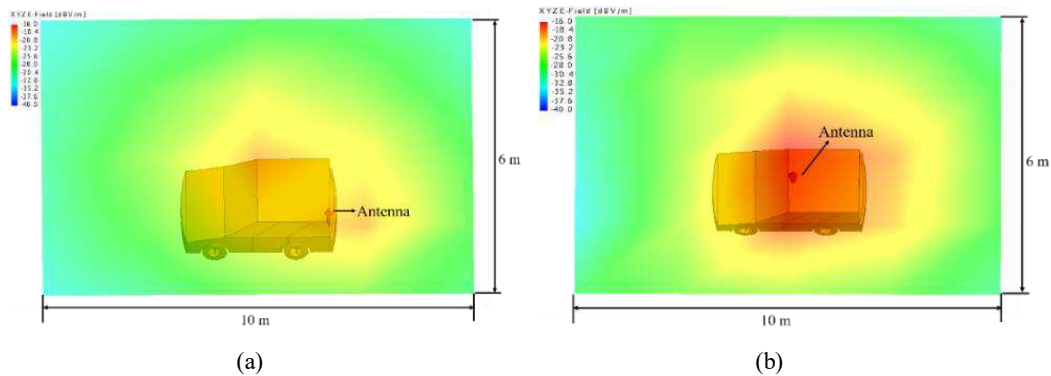
$$RSSI = 10 \log_{10}(P_{TRX}) - PL(\text{dB}) + G_a(\theta, \varphi) \quad (14)$$

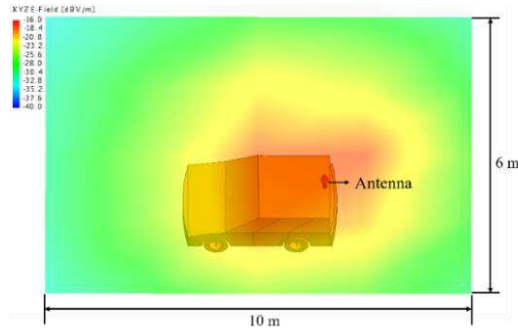
3.2 Results of radiation field simulation

Since the electromagnetic field distribution could be influenced by the shape and material of the vehicle body, the deployment of the vehicle antenna plays an important role on the final performance of the automobile antenna systems [20][21]. Moreover, the placement of the antenna is extremely limited due to aesthetic reasons defined by the automobile industry and the location of other electric equipment [22]. Three different versions of the automobile antennas on different roof configurations are investigated to evaluate the influence of antenna diagrams [23]. It is necessary to choose an appropriate position of automobile antennas to relieve these imperfect effects on radiation field

pattern.

The simulations of the installation positions of the automobile antenna are shown in Fig. 12, which discusses the electric field distributions of the antennas working at 2.64 GHz at different positions on the roof. Among them, the length of the car is 3 m, the width is 1.9 m, and the height is 1.8 m. And the surface of the car is made of metal. As shown in Fig. 12a, the antenna is installed in the corner of the roof, which causes imperfect radiation due to the refraction of the window glass and the diffraction of the sharp edge. When the antenna is installed in the center of front and rear roof shown in Fig. 12b and Fig. 12c, the electric field distributions are perfect, which can effectively achieve the vehicle communication. The vertical radiation patterns of antenna being placed in different positions on the roof at 2.64 GHz are shown in the Fig. 13. Pattern a denotes that the antenna is installed in the corner of the roof. Pattern b denotes that the antenna is installed in the center of front roof. Pattern c denotes that the antenna is installed in the center of rear roof. It is found that the pattern is severely distorted, if the antenna is installed in the corner of the roof. But the patterns of antenna being installed in the other two positions maintain good performance. Due to the requirements of automobile design and manufacture, the best installation position of the automobile antenna is the center of rear roof.





(c)

Fig. 12 Electric field distribution for different mounting positions of automobile antenna.

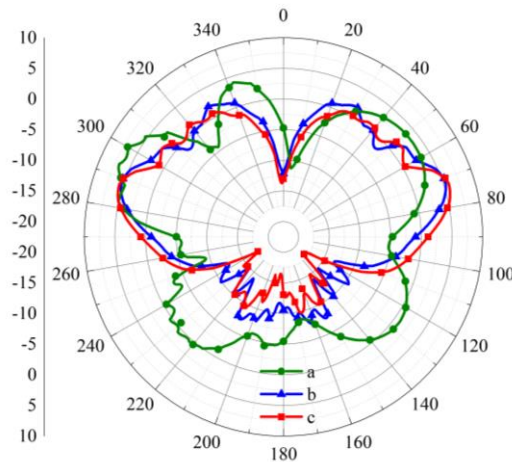


Fig. 13 The vertical radiation patterns with $\Phi=0^\circ$ of antennas being placed in different positions on the roof at 2.64 GHz.

An urban environment provides many challenges for V2V communications, including multiple propagation paths, buildings and other obstructions [24]. Figure.14 shows the simulation three-dimensional view of two automobile antennas in the urban. The propagation phenomenon of LOS and NLOS models have been simulated at 820 MHz to evaluate networking taking into account more realistic propagation conditions, as shown in Fig. 15. Two black stars indicate the positions of the two vehicles installed with the proposed automobile antennas. The area of the simulated urban environmental is 125 m \times 100 m, and the heights of the houses vary from 10 m to 12 m. The sufficient coverage is found in the red regions of electrical field distribution. The yellow and green areas show a slightly weak radiation due to the buildings which have a shadowing effect and diffraction on the electromagnetic wave propagation.

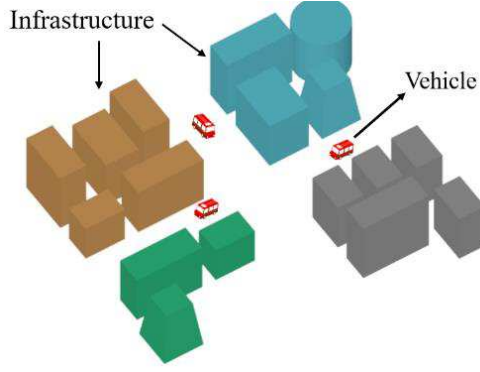


Fig. 14 The three-dimensional view of two automobile antennas in the urban.

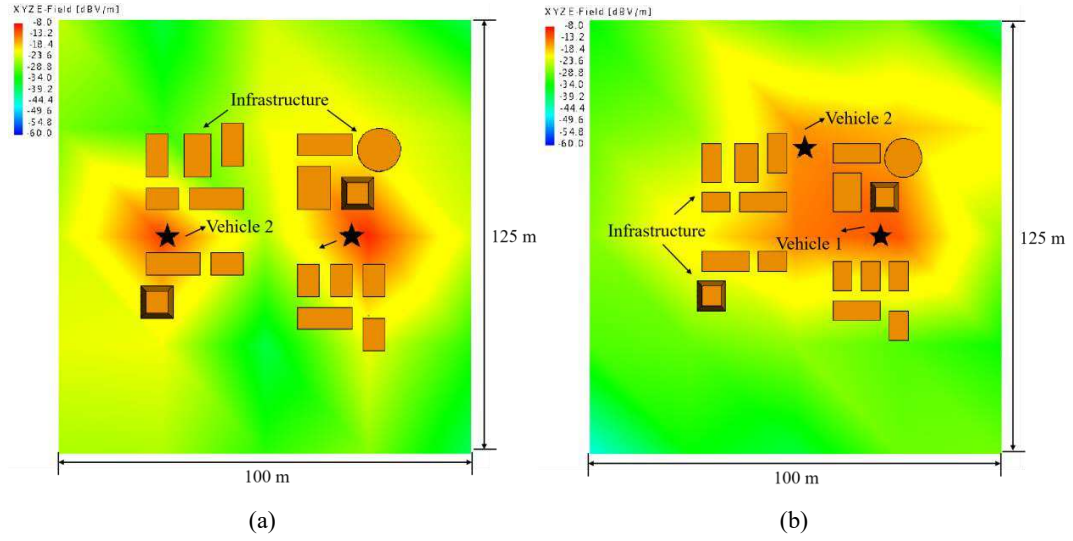


Fig. 15 Distribution of electrical field for two automobile antennas in the urban environment.

Diffraction occurs when the electromagnetic wave encounters sharp obstacles during propagation.

The reflected wave will propagate along the conical surface with the incident point as the vertex

[25]. The diffraction coefficient is

$$D_i = \frac{e^{j\frac{\pi}{4}}}{2(\pi k)^2 \sin \varepsilon} \left[\sec\left(\frac{1}{2}(\theta - \alpha)\right) \pm \csc\left(\frac{1}{2}(\theta + \alpha)\right) \right] \quad (15)$$

where ε is the incidence angle and α is the reflection angle. θ is the scattering angle. k is the wavenumber of electromagnetic wave. Although the electric field distribution is weak in some areas, the radiation of antennas can still cover every corner of the intersection.

The communication performance of V2V system is quantitatively evaluated with the simulated transmission coefficient of the two automobile antennas in the urban environment. The two vehicles

with the antennas are separated by the certain distance in the street, as shown in Fig. 16. The transmission coefficient varied with the propagation distance is shown in Fig. 17. The transmission coefficient of 820 MHz is obviously better than the one of 2.2 GHz, since the longer wavelength is conducive to electromagnetic wave propagation in the environment of densely distributed buildings. The transmission coefficient of antenna shows low attenuation with the increasing of the distance. Therefore, the automobile antenna can realize long-distance communication.

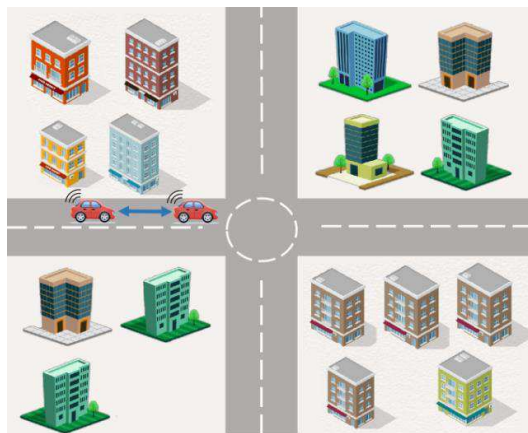


Fig. 16 Schematic diagram of the automobile antenna in the urban environment.

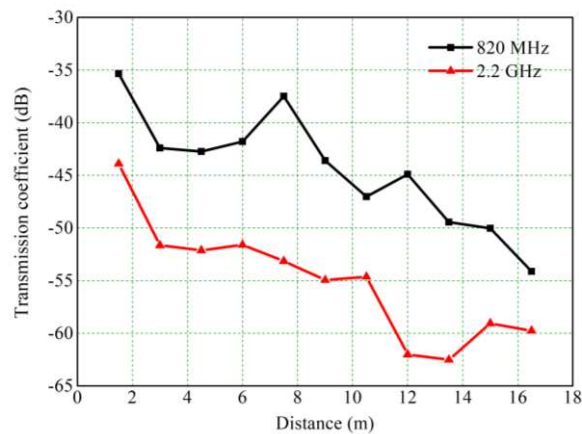


Fig. 17 Transmission coefficients for different operation bands of the automobile antenna in the urban environment.

4 Coverage extending for the mobile communication network

4.1 Principle of coverage extending with the automobile antenna

The scenario of one operator's infrastructure serving multiple vehicles is considered in the IoV

systems, as shown in Fig. 18. The infrastructure services are provided for the V2V system by various communication operators. Since the operators use different authorization frequencies, the vehicles communicate with each other in the public land mobile network (PLMN) when the infrastructures of multiple operators serve different vehicles.

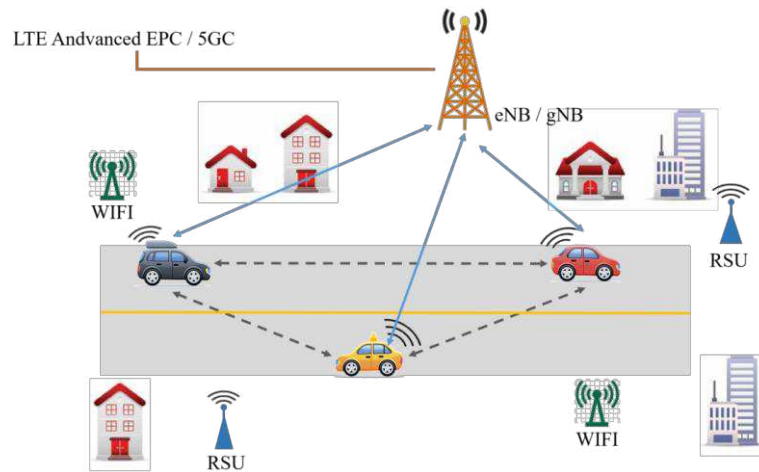


Fig. 18 Internet of vehicles schematic diagram.

The vehicles receive the information from the enhanced Node B (eNB) or the generation Node B (gNB) when the vehicles are in the service area [26][27]. Meanwhile, the vehicles upload data, such as location information, movement speed, destination, etc. There is also data interaction between the vehicles, and the vehicles communicate with RSU and WiFi unit. The eNB/gNB upload the data to Evolved Packet Cor (EPC) or 5G Core (5G C) for data analysis and processing. Due to the multiple connections between the vehicles and nodes, the vehicles are required to be equipped with a variety of interfaces and the high-quality transceiver devices.

Due to the influence of the terrain and buildings, there are some blind areas in the coverage of the eNB/gNB, which could lead to communication interruption. In addition, the gNB uses high frequency bands, which decreases the coverage area. A method of using the automobile antenna as mobile micro node is proposed to extend the communication coverage, as shown in Fig. 19. The

multiple interfaces of the vehicle could be used to connect with the eNB/gNB in the IoV system, and the vehicle can be used as a mobile micro node of the radio access net (RAN).

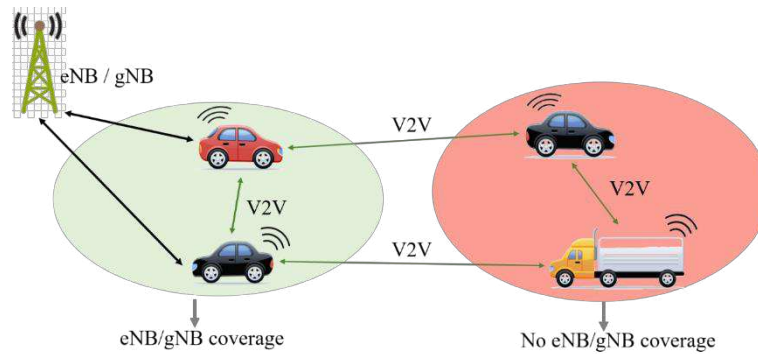


Fig. 19 Vehicle antenna as micro node.

4.2 Simulation results of coverage extending solution

The coverage of the gNB is simulated in the urban environment, as shown in Fig. 20 and Fig. 21. The building heights are form 8 m to 12 m, and the black triangle is the location of the gNB. The height of gNB is 25 m and the direction angle is 80° . And the gNB is set at a downward angle of 10° in the single sector case working at 1.8 GHz. The vehicles could communicate fluently with each other in the area close to the gNB. The blind area is also found in the service area, which is caused by the shadowing effect of buildings. As a consequence, the user experience will be relatively poor and the vehicles will even disconnect in the blind area.

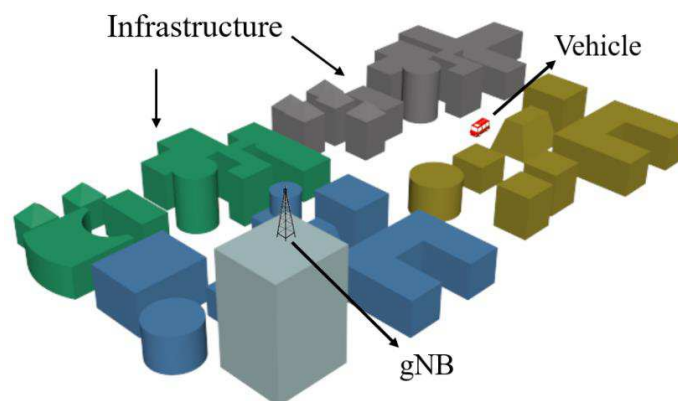


Fig. 20 The three-dimensional view of simulating gNB of single sector coverage in urban.

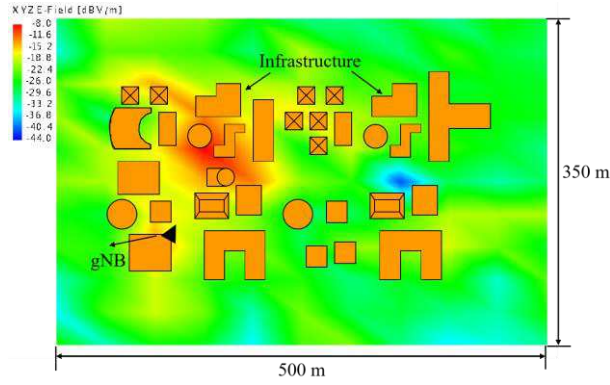


Fig. 21 Distribution map of gNB of single sector coverage in urban environment.

The location of the vehicle with the automobile antenna working at 3.42 GHz is marked as the pentagram, as shown in Fig. 22. When the vehicle with PC5 interfaces drives into the blind area, the transceiver on the vehicle could act as a mobile micro node. The V2X communication in the area will be significantly improved. Thus, the civil vehicle can be used as communication emergency vehicle to improve the coverage shortage in the urban environment.

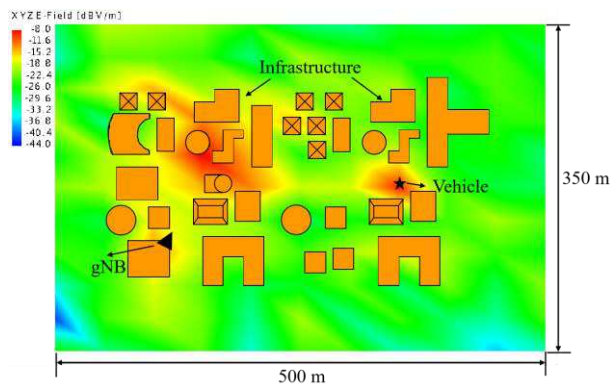


Fig. 22 Supplementary effect drawing of blind area of mobile station for vehicle communication.

5 Discussion

A novel automobile antenna working in a broadband frequency is proposed. The antenna obtains the good omnidirectional radiation pattern and the impedance matching without any additional matching network, which are improved by loading the toothed capacitor and the impedance matching disc. The electric field distribution and transmission coefficient of the antenna installed on the vehicle roof are simulated, which shows high gain with low loss. The good omnidirectional

radiation performance enables the antenna to effectively connect the mobile cellular networks and the IoV systems. Therefore, the network coverage performance is improved by the automobile antenna. Since the antenna without any additional matching network, the whole antenna structure is compact and easy to be installed on the top of the vehicle. Due to the high reliability and low cost, the proposed automobile antenna could be widely used for the V2X communication system.

Abbreviations

IoV: Internet of vehicles; IoT: Internet of things; LTE: Long Term Evolution; 5G: 5th generation wireless systems; DSRC: dedicated short-range communication; V2V: vehicle to vehicle; V2I: vehicle to infrastructure; V2X: vehicle to everything; MBD: main beam direction; eNB: enhanced Node B; gNB: generation Node B; EPC: Evolved Packet Cor

Acknowledgements

Not applicable.

Authors' contributions

All the authors were involved in the writing of the manuscript. All authors have given approval to the final version of the manuscript.

Funding

This work was supported by the Chongqing Basic Science and Frontier Technology Research Project (cstc2017jcyjAX0193) and the National Natural Science Foundation of China [grant No. 61871063].

Availability of data and materials

The datasets used and/or analyzed during the current study are available from the corresponding author on reasonable request.

Competing interests

The authors declare that they have no competing interests.

Author details

¹College of Electronic Engineering, Chongqing University of Posts and Telecommunications, Chongqing 400065, China. ²Electronic Information and Networking Research Institute, Chongqing University of Posts and Telecommunications, Chongqing 400065, China.

References

1. S. Hastürkoğlu, S. Lindenmeier, in 2017 11th European Conference on Antennas and Propagation (EuCAP). A wideband automotive antenna for actual and future mobile communication 5G/LTE/WLAN with low profile (IEEE, 2017), pp. 602-605. doi: 10.23919/EuCAP.2017.7928669.

2. I. Goncharova, S. Lindenmeier, in 2014 8th European Conference on Antennas and Propagation (EuCAP). A high-efficient 3-D Nefer-antenna for LTE communication on a car (IEEE, 2014), pp. 3273-3277. doi:10.1109/EuCAP.2014.6902527.
3. S. Kim, D. Kang, J. Choi, in 2017 International Symposium on Antennas and Propagation (ISAP). Beam reconfigurable antenna using switchable parasitic elements for V2V applications (IEEE, 2017), pp. 1-2. doi:10.1109/ISANP.2017.8229006.
4. H. Wong, K. K. So, X. Gao, Bandwidth enhancement of a monopolar patch antenna with V-shaped slot for Car-to-Car and WLAN communications. IEEE Trans. Vehi. Tech. 65(3), 1130-1136 (2016). doi:10.1109/TVT.2015.2409886.
5. W. Sung, T. Chuang, J. Chen, K. Chang, in 2015 International Conference on Computational Intelligence and Communication Networks (CICN). IOT-type cloud online real-time multi-car localization and communication system (IEEE, 2015), pp. 913-917. doi:10.1109/CICN.2015.180.
6. D. N. Chowdhury, N. Agarwal, A. B. Laha, A. Mukherjee, in 2018 Second International Conference on Electronics, Communication and Aerospace Technology (ICECA). A Vehicle-to-Vehicle communication system using IOT approach (IEEE, 2018), pp. 915-919. doi:10.1109/ICECA.2018.8474909.
7. A. Gharsallah, N. Omheni, K. Ghanmi, F. Zarai, M. Neji, in 2017 IEEE/ACS 14th International Conference on Computer Systems and Applications (AICCSA). A seamless mobility mechanism for V2V communications (IEEE, 2017), pp.1063-1069. doi:10.1109/AICCSA.2017.109.
8. K. Abboud, H. A. Omar, W. Zhuang, Interworking of DSRC and cellular network technologies

- for V2X communications: A Survey. *IEEE Trans. Vehic. Tech.* 65(12), 9457-9470 (2016).
doi:10.1109/TVT.2016.2591558.
9. O. Kwon, R. Song, B. Kim, A fully integrated Shark-Fin antenna for MIMO-LTE, GPS, WLAN, and WAVE applications. *IEEE Ant. Wirel. Propa. Let.* 17(4), 600-603 (2018).
doi:10.1109/LAWP.2018.2805681.
 10. K. Xu, H. Luyen and N. Behdad, A Decoupling and Matching Network Design for Single- and Dual-Band Two-Element Antenna Arrays, in *IEEE Transactions on Microwave Theory and Techniques*.
 11. Y. J. Guo , K. D. Xu , X. H. Tang . Multi-Functional Ultra-Wideband Monopole Antenna with High Frequency Selectivity. *Appl. Comput. Electrom. Society Newsletter*, 33(1), 37-42 (2018).
 12. Y. Guo, X. Tang, K. D. Xu, Ai, Jing, Dual high-selectivity band-notched UWB monopole antenna using simple dual-mode resonator and high-impedance lines. *Int. J. Microw. Wirele. Tech.* 9(04), 923–929 (2017).
 13. M. A. B. Diez, S. Lindenmeier, in 2015 IEEE International Symposium on Antennas and Propagation & USNC/URSI National Radio Science Meeting. A highly efficient Car2Car multiband rooftop automotive antenna (IEEE, 2015), pp. 1606-1607. doi: 10.1109/APS.2015.7305192.
 14. M. Gallo, S. Bruni, M. Pannozzo, D. Zamberlan, in 2013 7th European Conference on Antennas and Propagation (EuCAP). Performance evaluation of C2C antennas on car body (IEEE, 2013), pp. 3136-3139.
 15. N. Guan, H. Chiba, Y. Yamaguchi, Y. Niihara, H. Tayama, in 2014 IEEE-APS Topical Conference on Antennas and Propagation in Wireless Communications (APWC). A flat roof

- automobile antenna module for LTE, GPS and SDARS applications (IEEE, 2014), pp. 11-14.
doi: 10.1109/APWC.2014.6905517.
16. E. Ghafari, A. Fuchs, D. Eblenkamp, D. N. Aloï, in 2014 IEEE-APS Topical Conference on Antennas and Propagation in Wireless Communications (APWC). A vehicular rooftop, Shark-fin, multiband antenna for the GPS/LTE/Cellular/DSRC systems (IEEE, 2014), pp. 237-240.
doi: 10.1109/APWC.2014.6905546.
 17. M. Geissler, K. Scharwies, J. Christ, in 2014 German Microwave Conference (GeMiC). Intelligent antenna systems for cars (IEEE, 2014) pp. 1-3.
 18. N. D. Chatzidiamantis, H. G. Sandalidis, G. K. Karagiannidis, in International Conference on Communications and Information Technology (ICCIT). On the inverse-Gaussian shadowing (IEEE, 2011), pp.142-146. doi:10.1109/ICCITECHNOL.2011.5762666.
 19. A. Ghazal, Y. Yuan, C. X. Wang, A Non-Stationary IMT-Advanced MIMO channel model for High-Mobility wireless communication systems. IEEE Trans. Wirel. Commun. 16(4): 2057-2068 (2017). doi: 10.1109/TWC.2016.2628795.
 20. S. Lindenmeier, I. Goncharova, S. Hastürkoğlu, M. B. Diez, in IEEE-APS Topical Conference on Antennas and Propagation in Wireless Communications (APWC). Antennas for terrestrial communication in vehicles and their interaction with antennas for satellite services (IEEE, 2017), pp. 334-337. doi: 10.1109/APWC.2017.8062319.
 21. E. Whalen, A. Elfrgani. C. Reddy, R. Rajan, in 2018 IEEE International Symposium on Antennas and Propagation and USNC/URSI National Radio Science Meeting. Antenna placement optimization for Vehicle-To-Vehicle communications (IEEE, 2018), pp. 1673-1674,
doi:10.1109/apusncursinrsm.2018.8609047.

22. M. B. Diez, P. Plitt, W. Pascher, in 2015 the 45th European Microwave Conference (EuMC).
Antenna placement and wave propagation for Car-to-Car communication (IEEE, 2015), pp. 207-210. doi: 10.1109/EuMC.2015.7345736.
23. A. Kwoczek, Z. Raida, J. Lacik, in 2011 IEEE Vehicular Networking Conference (VNC).
Influence of car panorama glass roofs on Car2Car communication (IEEE, 2011), pp. 246-251.
doi: 10.1109/VNC.2011.6117107.
24. S. Biddlestone, K. Redmill, R. Miucic, An integrated 802.11p WAVE DSRC and vehicle traffic simulator with experimentally validated urban (LOS and NLOS) propagation models. IEEE Trans. Intel. Tran. Syst. 13(4): 1792-1802 (2012). doi: 10.1109/TITS.2012.2213816.
25. Q. Zhan, Y. Fang, M. Zhuang, M. Yuan, Q. H. Liu, Stabilized DG-PSTD Method With Nonconformal Meshes for Electromagnetic Waves. IEEE Trans. Antennas Propag. 68(6), 4714-4726 (2020).
26. D. Kombate, Wanglina, in 2016 IEEE International Conference on Internet of Things (iThings) and IEEE Green Computing and Communications (GreenCom) and IEEE Cyber, Physical and Social Computing (CPSCoM) and IEEE Smart Data (SmartData). The Internet of vehicles based on 5G communications (IEEE, 2016). doi: 10.1109/iThings-GreenCom-CPSCoM-SmartData.2016.105
27. Y. Zhang, R. Wang, M. S. Hossain, M. F. Alhamid, M. Guizani, Heterogeneous information Network-Based content caching in the Internet of Vehicles. IEEE Trans. Vehic. Tech. 68(10), 10216-10226 (2019). doi: 10.1109/TVT.2019.2936792.

Figure Title and Legend

Figure 1 Various V2X scenarios in IoT systems. The V2V network is composed of the vehicles

connected to each other. The vehicles also communicate with the infrastructure and pedestrian to form V2I and V2P. The V2N network could be the subsystem of mobile communication system.

Figure 2 Schematic diagram of simple antenna radiator. The monopole antenna is placed on the infinite ground. The far radiation field is orthogonal decomposed into E_{θ} and E_{φ} .

Figure 3 Three kinds of rooftop antennas with different performance. (a) Antenna with toothed capacitor and L-shaped capacitor. (b) Antenna with impedance matching disc. (c) The proposed wide band antenna structure.

Figure 4 The electrical current distributions of the proposed wide band antenna structure at different frequencies. (a) The electrical current distribution at 900 MHz. (b) The electrical current distribution at 3 GHz.

Figure 5 Input impedance of three kinds of rooftop antennas with different performance. (a) Real part of input impedance. (b) Imaginary part of input impedance.

Figure 6 S parameters of the rooftop antennas. Although all of the three types of antennas could meet the requirement of LTE low frequency band, the 5G frequency band could only be covered by the antenna (c).

Figure 7 The radiation pattern of antenna at 790 MHz. (a) Vertical radiation pattern. (b) Horizontal radiation pattern.

Figure 8 The radiation pattern of antenna at 2.64 GHz. (a) Vertical radiation pattern. (b) Horizontal radiation pattern.

Figure 9 The radiation pattern of antenna at 3.42 GHz. (a) Vertical radiation pattern. (b) Horizontal radiation pattern.

Figure 10 The radiation pattern of antenna at 4.42 GHz. (a) Vertical radiation pattern. (b) Horizontal radiation pattern.

radiation pattern.

Figure 11 The radiation pattern of antenna at 5.41 GHz. (a) Vertical radiation pattern. (b) Horizontal radiation pattern.

Figure 12 Electric field distribution for different mounting positions of automobile antenna. (a) Antenna is installed in the corner of the roof. (b) Antenna is installed in the center of the roof. (c) Antenna is installed at the rear edge of the roof.

Figure 13 The vertical radiation patterns with $\Phi=0^\circ$ of the antenna being placed in different positions on the roof at 2.64 GHz. Line a is the radiation pattern of antenna installed in the corner of the roof. Line b is the radiation pattern of antenna installed in the center of the roof. Line c is the radiation pattern of antenna installed at the rear edge of the roof.

Figure 14 The three-dimensional view of simulating distribution of electrical field for two automobile antennas in the urban.

Figure 15 Distribution of electrical field for two automobile antennas in the urban environment. (a) LOS environment. (b) NLOS environment.

Figure 16 Schematic diagram of the automobile antenna in the urban environment. The two vehicles loaded with the automobile antenna communicate with each other, and the propagation distance varies with the relative motion.

Figure 17 Transmission coefficients for different operation bands of the automobile antenna in the urban environment. The red line is the 2.2 GHz frequency band, and the black line is the 820 MHz frequency band.

Figure 18 Internet of vehicles schematic diagram. The transceivers on the vehicles could be the extended RAN nodes for the eNB/gNB.

Figure 19 Vehicle antenna as micro node. The coverage of mobile communication is improved with the automobile antenna.

Figure 20 The three-dimensional view of simulating gNB of single sector coverage in urban.

Figure 21 Distribution map of gNB of single sector coverage in urban environment. There is apparent blind area, which is caused by the large-scale fading.

Figure 22 Supplementary effect drawing of blind area of mobile station for vehicle communication. The blind area is perfectly eliminated by the proposed automobile antenna.

Figures

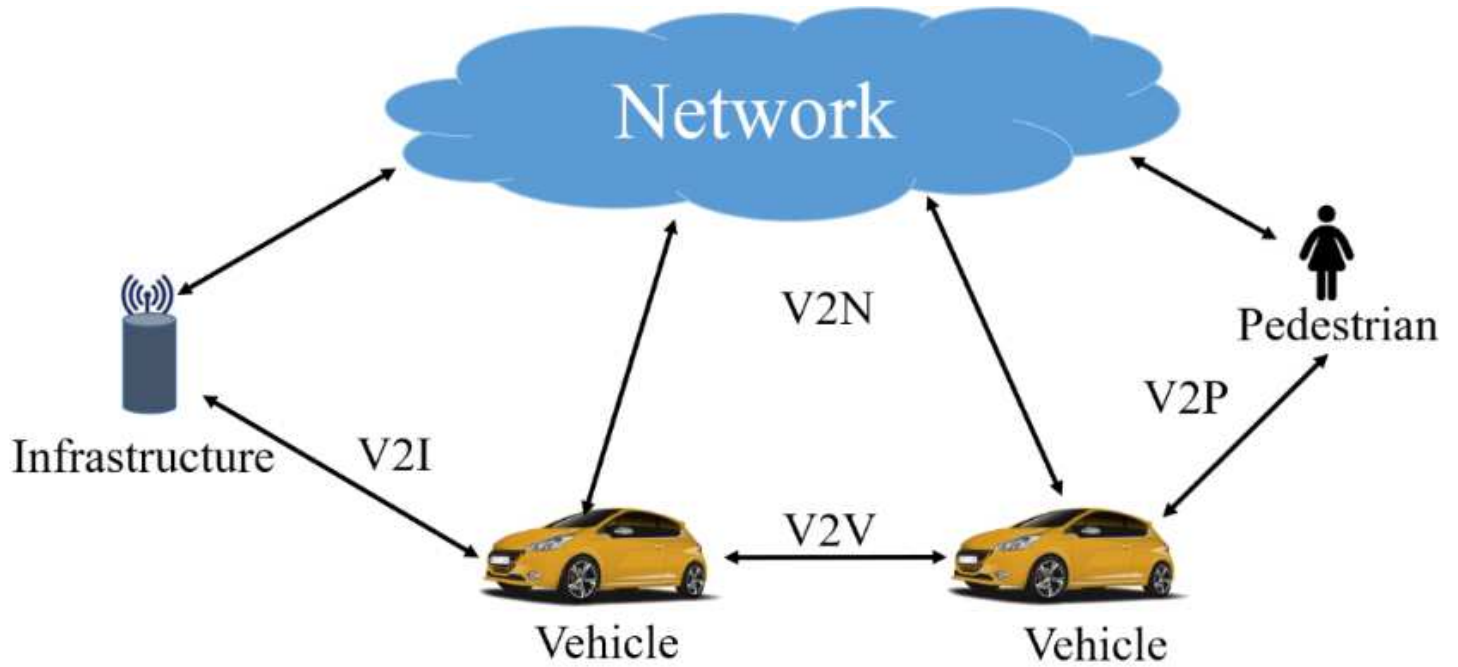


Figure 1

Various V2X scenarios in IoT systems.

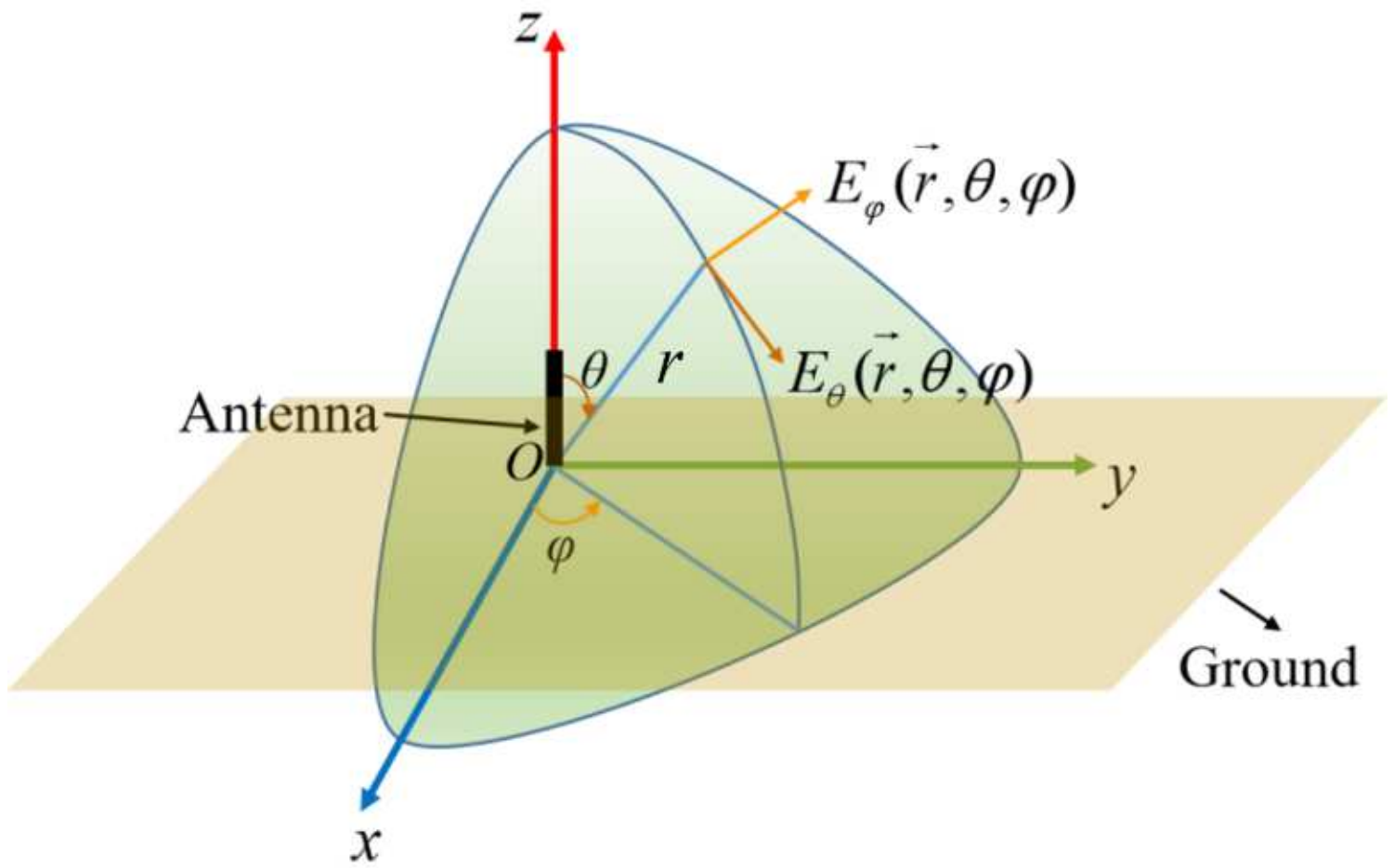


Figure 2

Schematic diagram of simple antenna radiator.

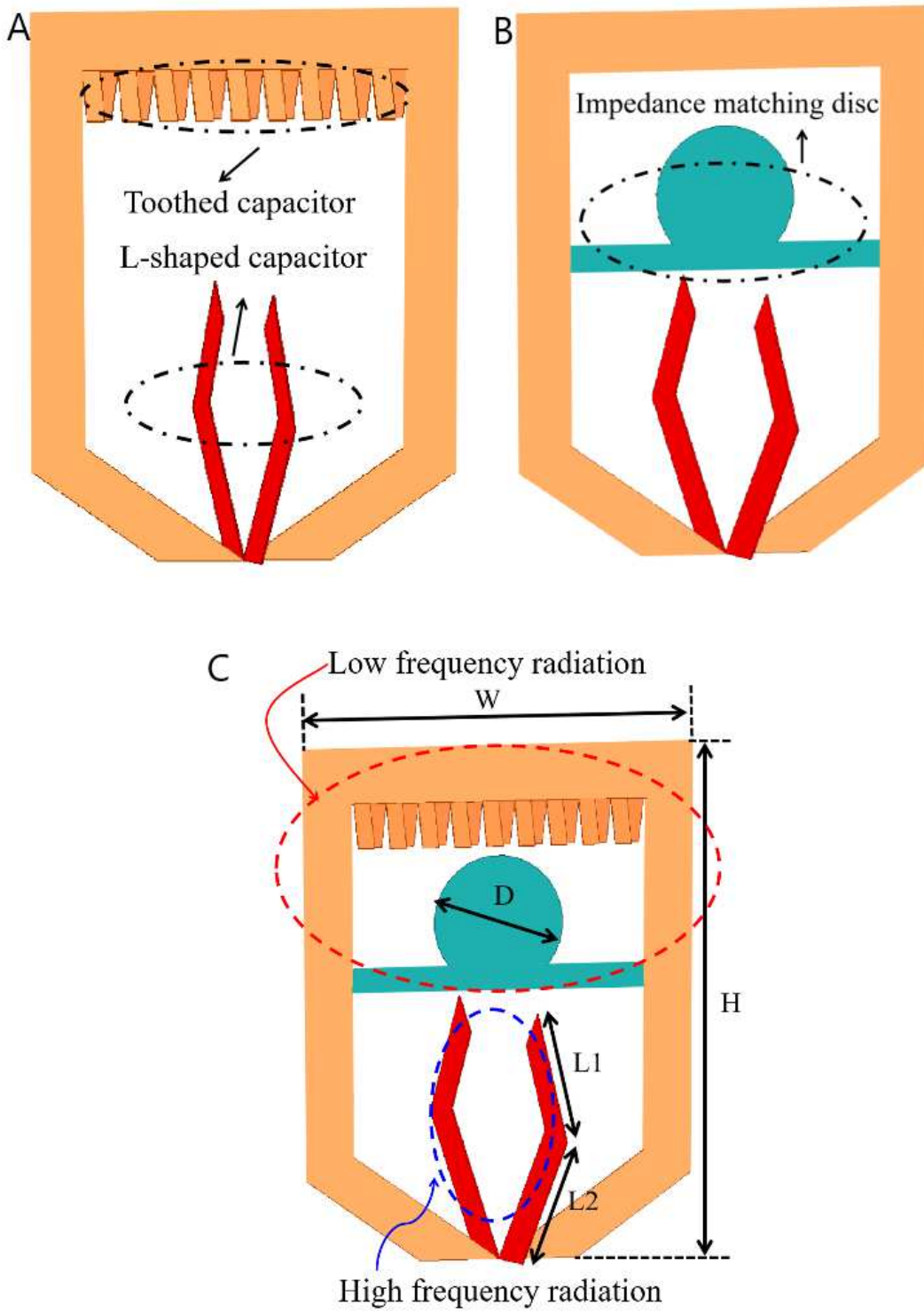


Figure 3

Three kinds of rooftop antennas with different performance.

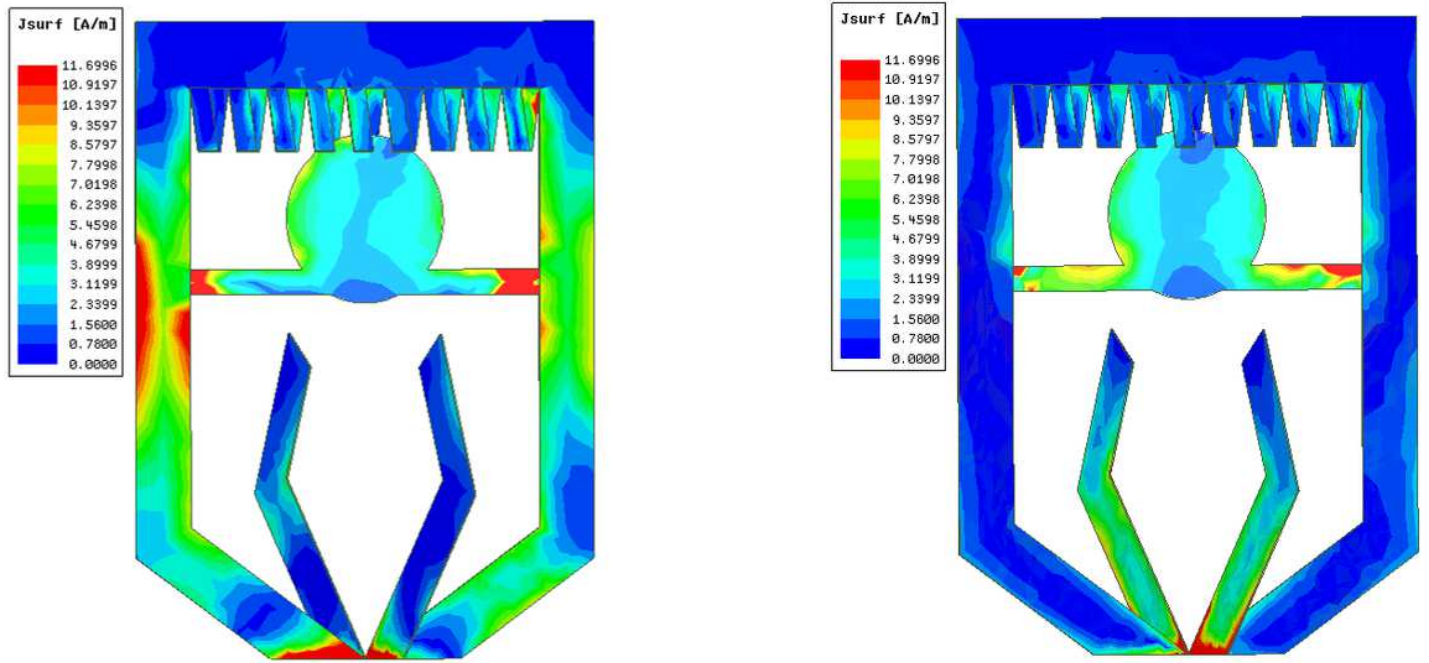


Figure 4

The electrical current distributions at different frequencies.

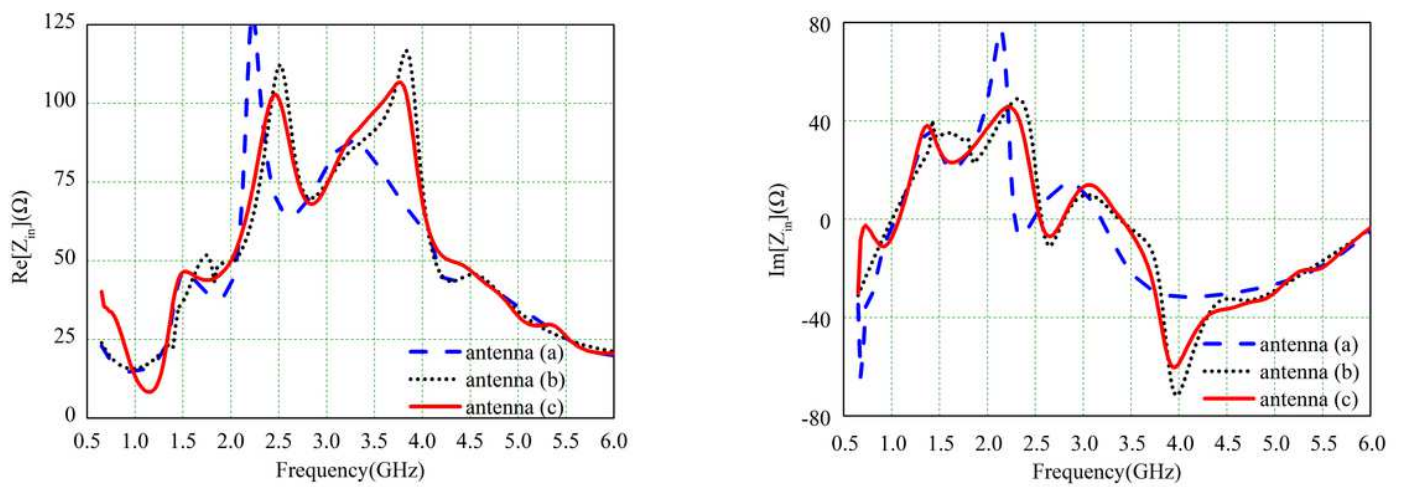


Figure 5

Input impedance of the antennas.

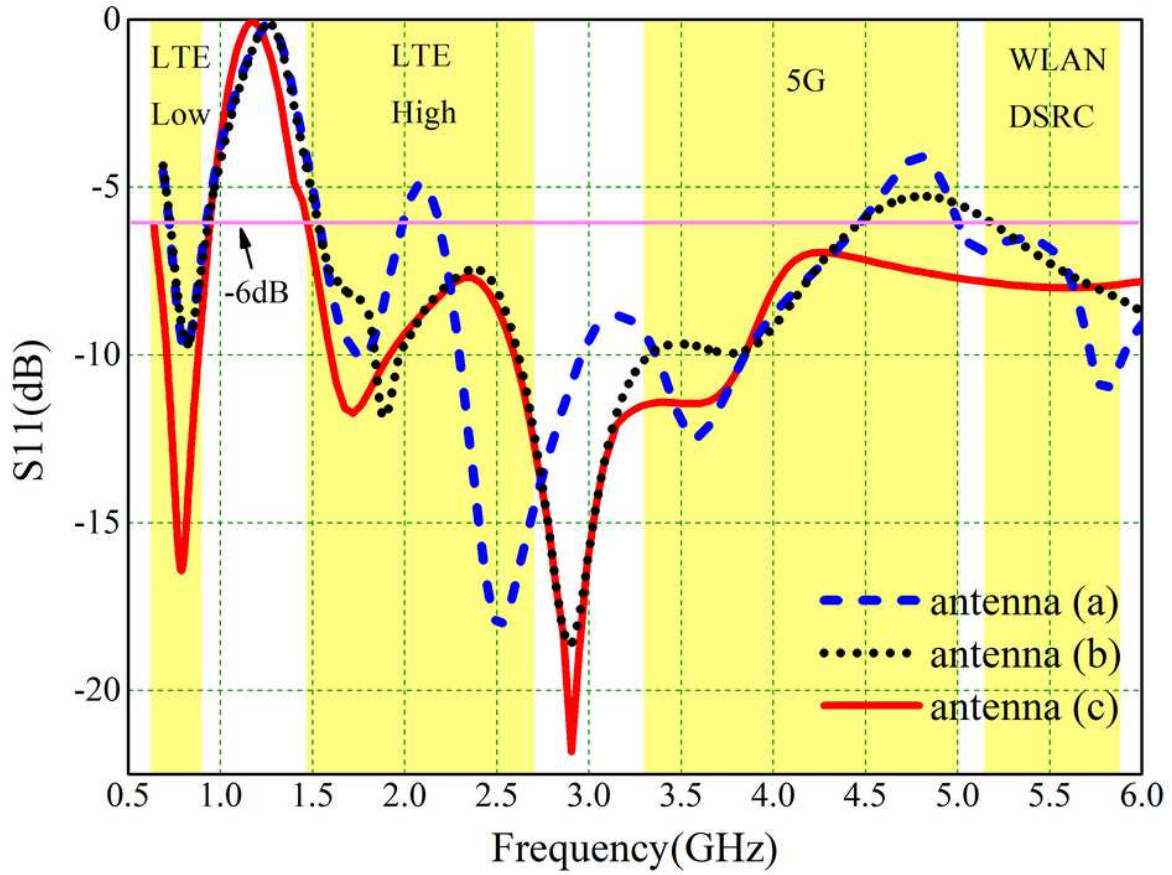


Figure 6

S parameters of the rooftop antennas.

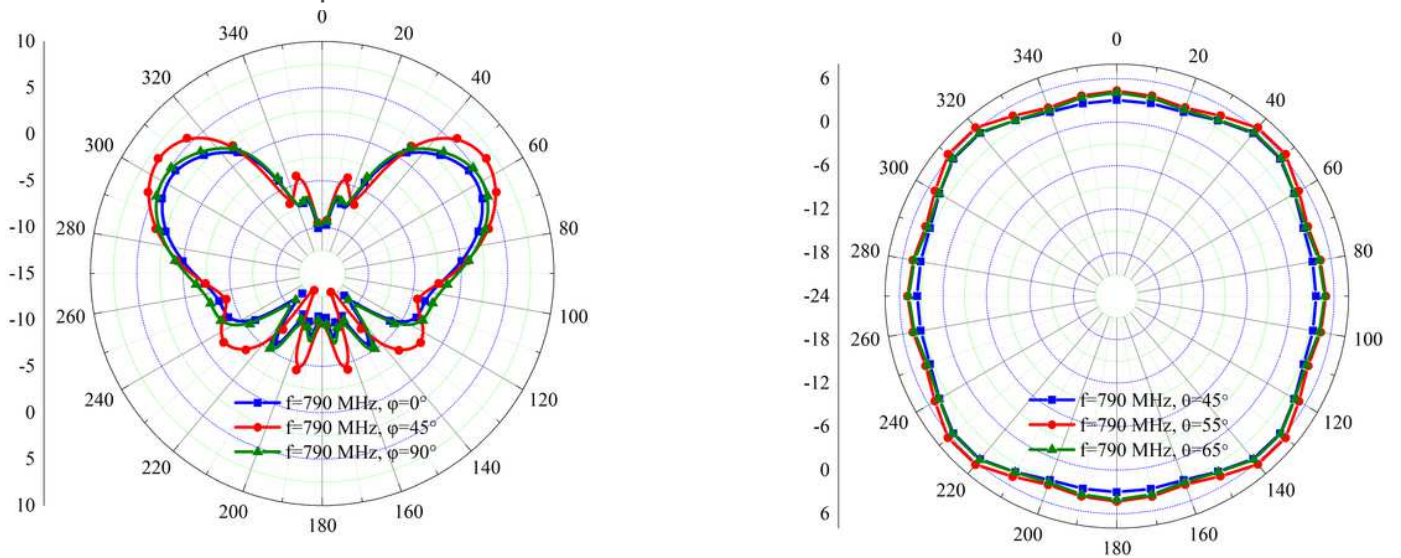


Figure 7

The radiation pattern of antenna at 790 MHz.

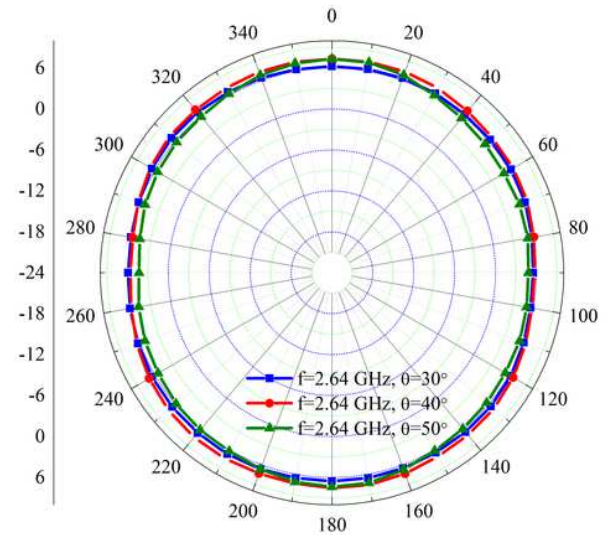
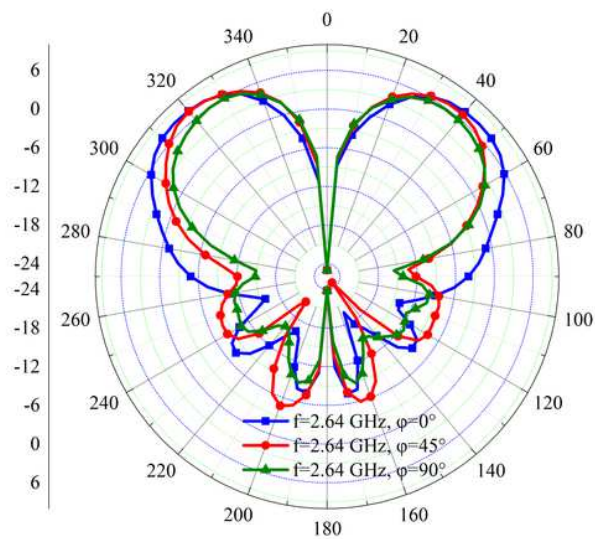


Figure 8

The radiation pattern of antenna at 2.64 GHz.

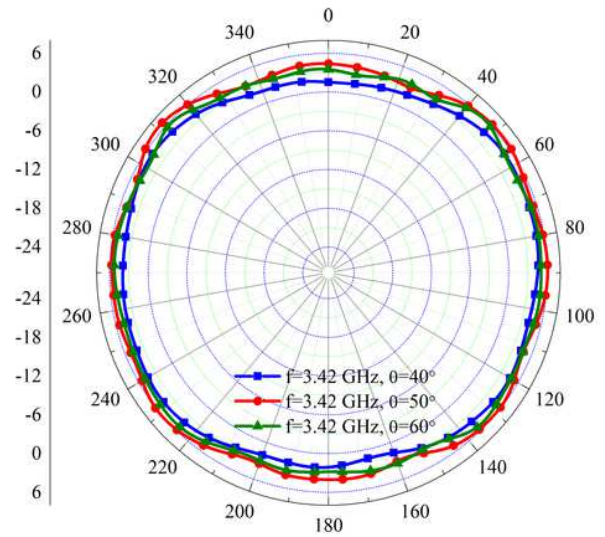
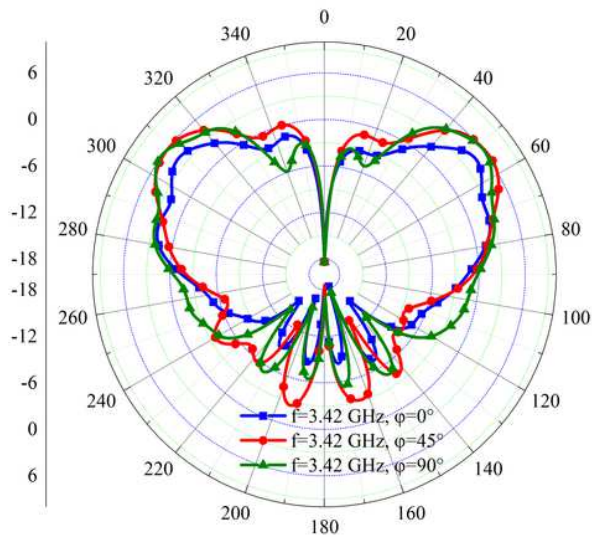


Figure 9

The radiation pattern of antenna at 3.42 GHz.

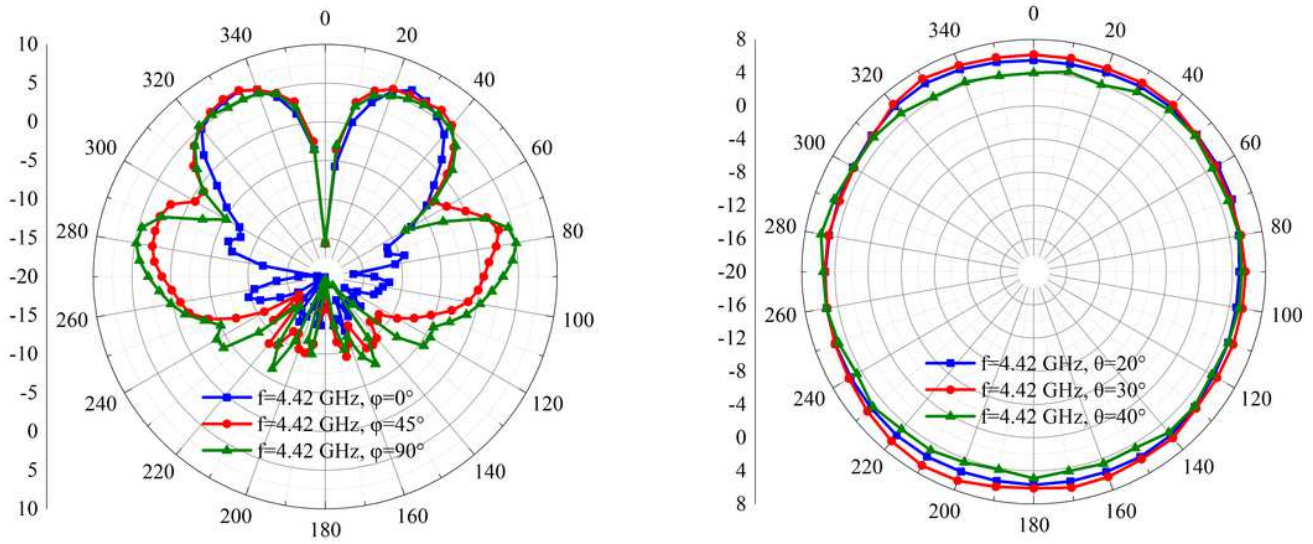


Figure 10

The radiation pattern of antenna at 4.42 GHz.

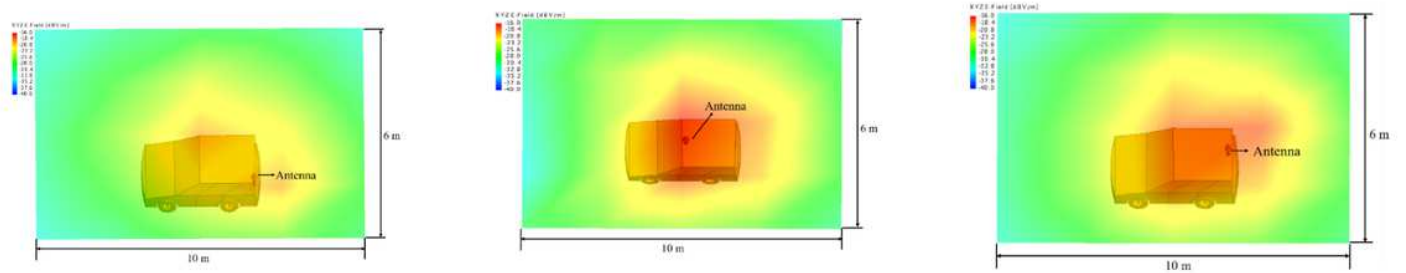


Figure 11

Electric field distribution for different mounting positions of automobile antenna.

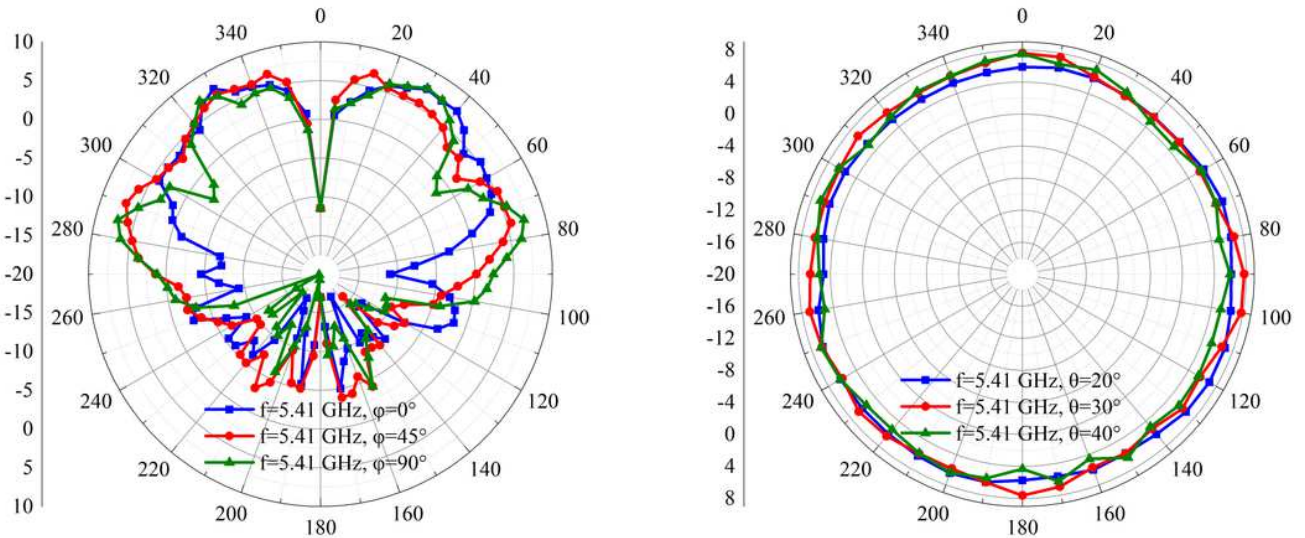


Figure 12

The radiation pattern of antenna at 5.41 GHz.

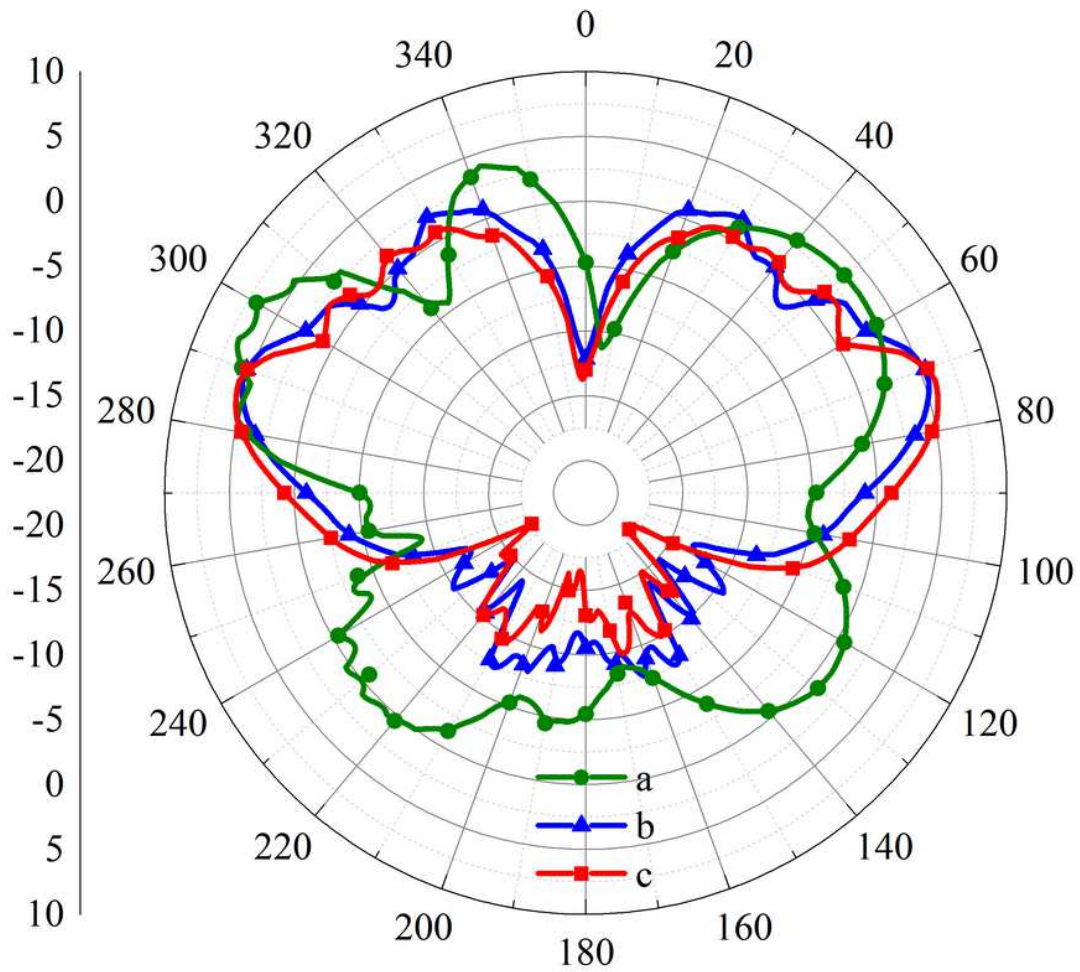


Figure 13

The vertical radiation patterns with $\Phi=0^\circ$ of antennas being placed in different positions on the roof at 2.64 GHz.

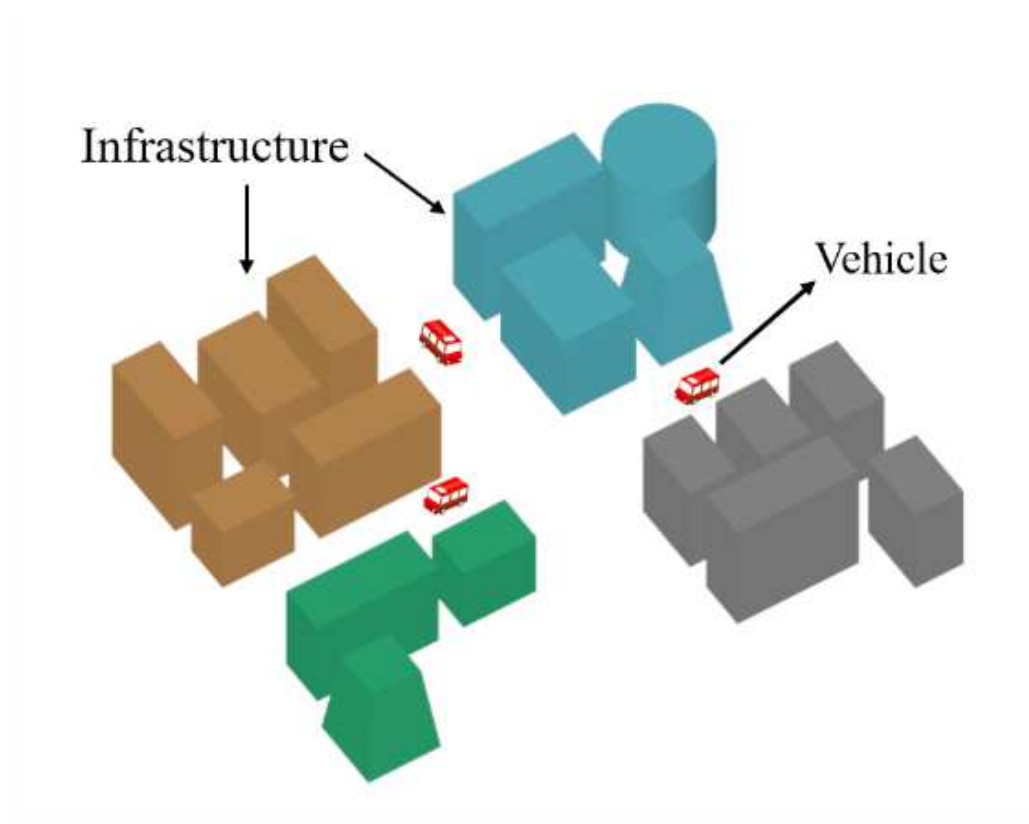


Figure 14

The three-dimensional view of two automobile antennas in the urban.

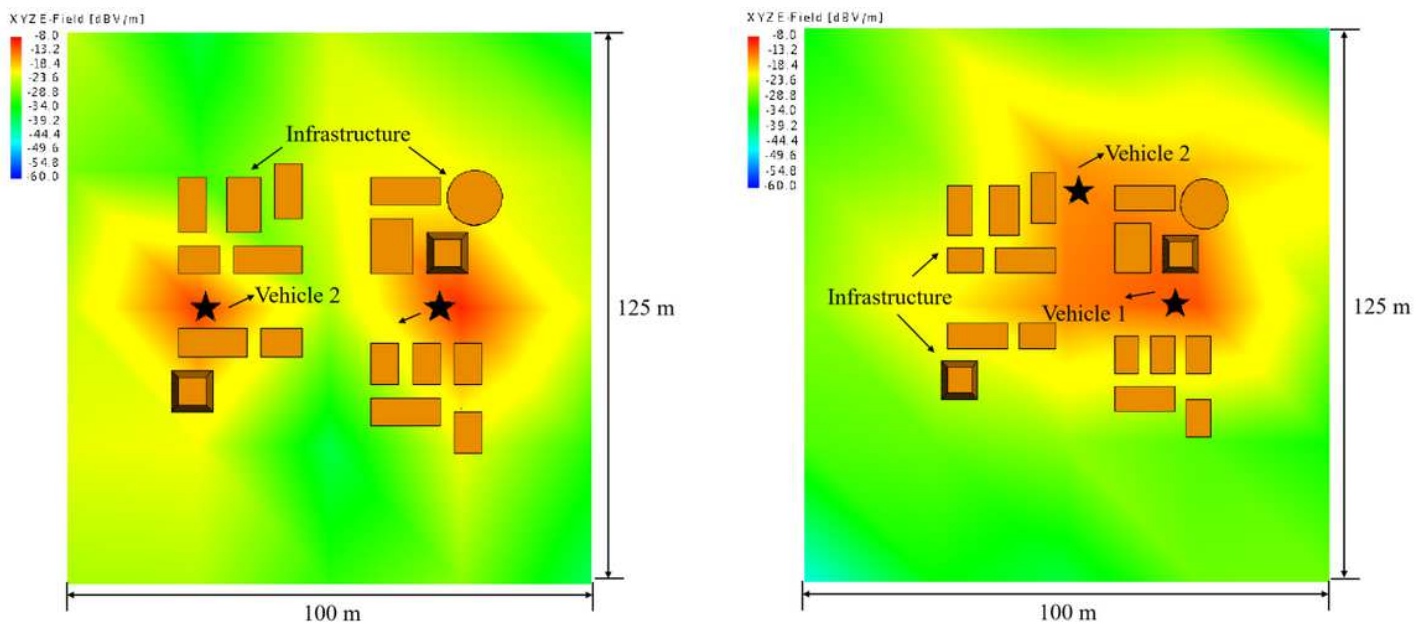


Figure 15

Distribution of electrical field for two automobile antennas in the urban environment.

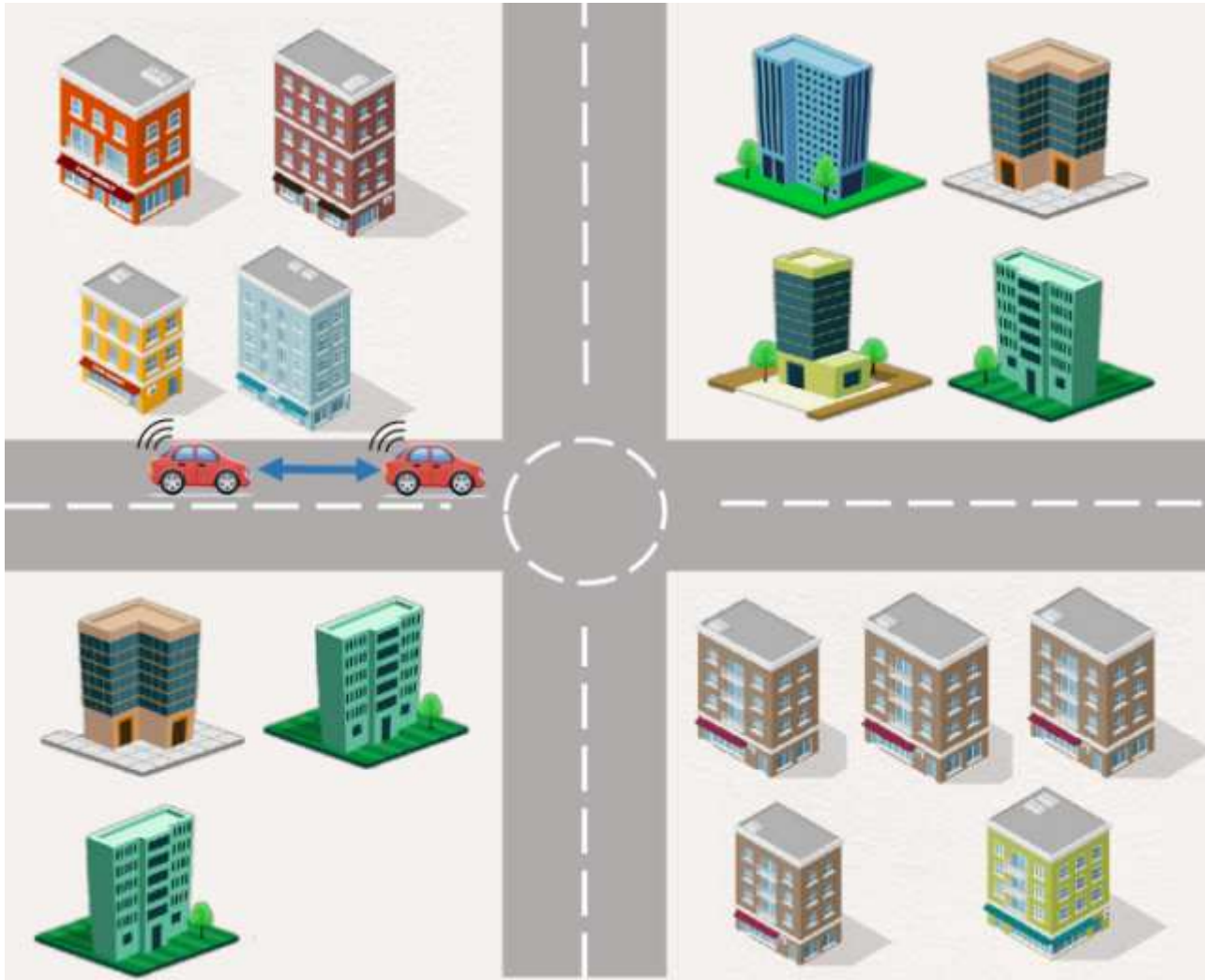


Figure 16

Schematic diagram of the automobile antenna in the urban environment.

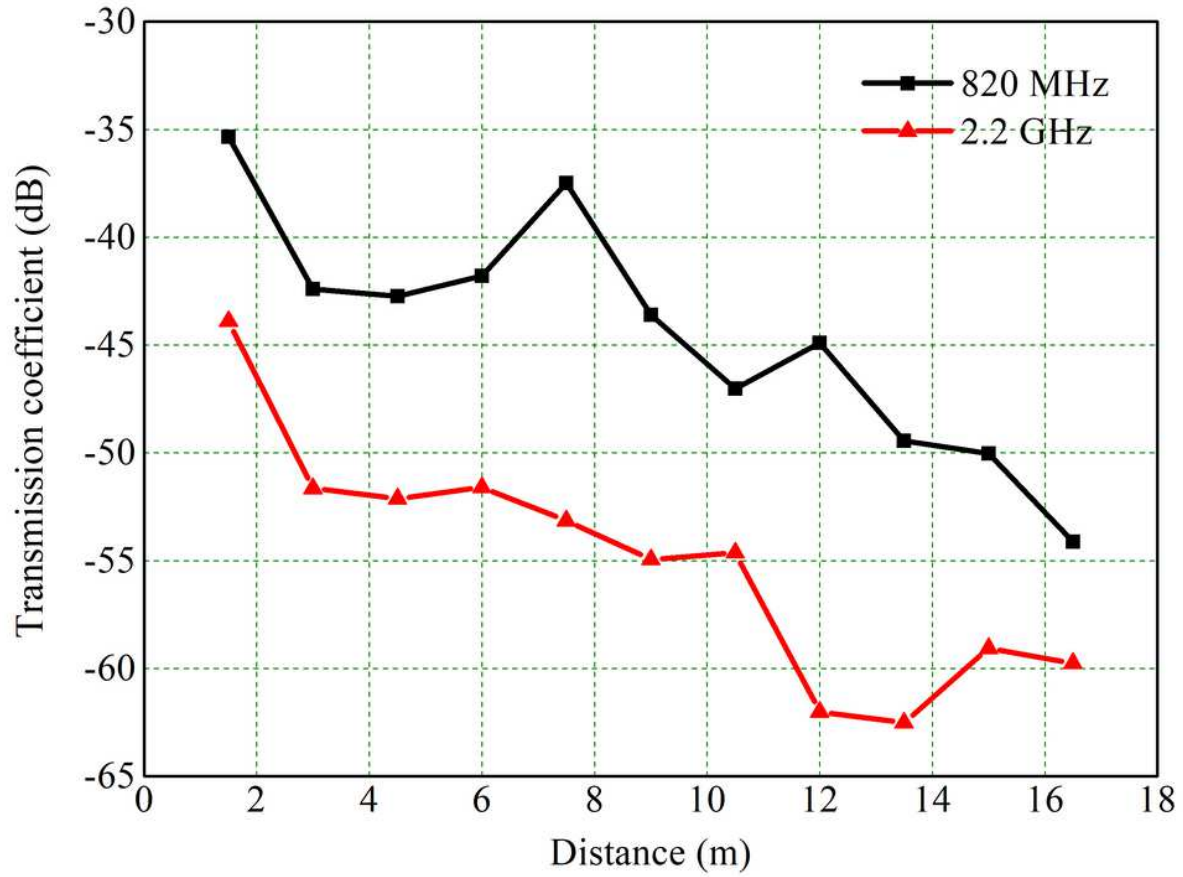


Figure 17

Transmission coefficients for different operation bands of the automobile antenna in the urban environment.

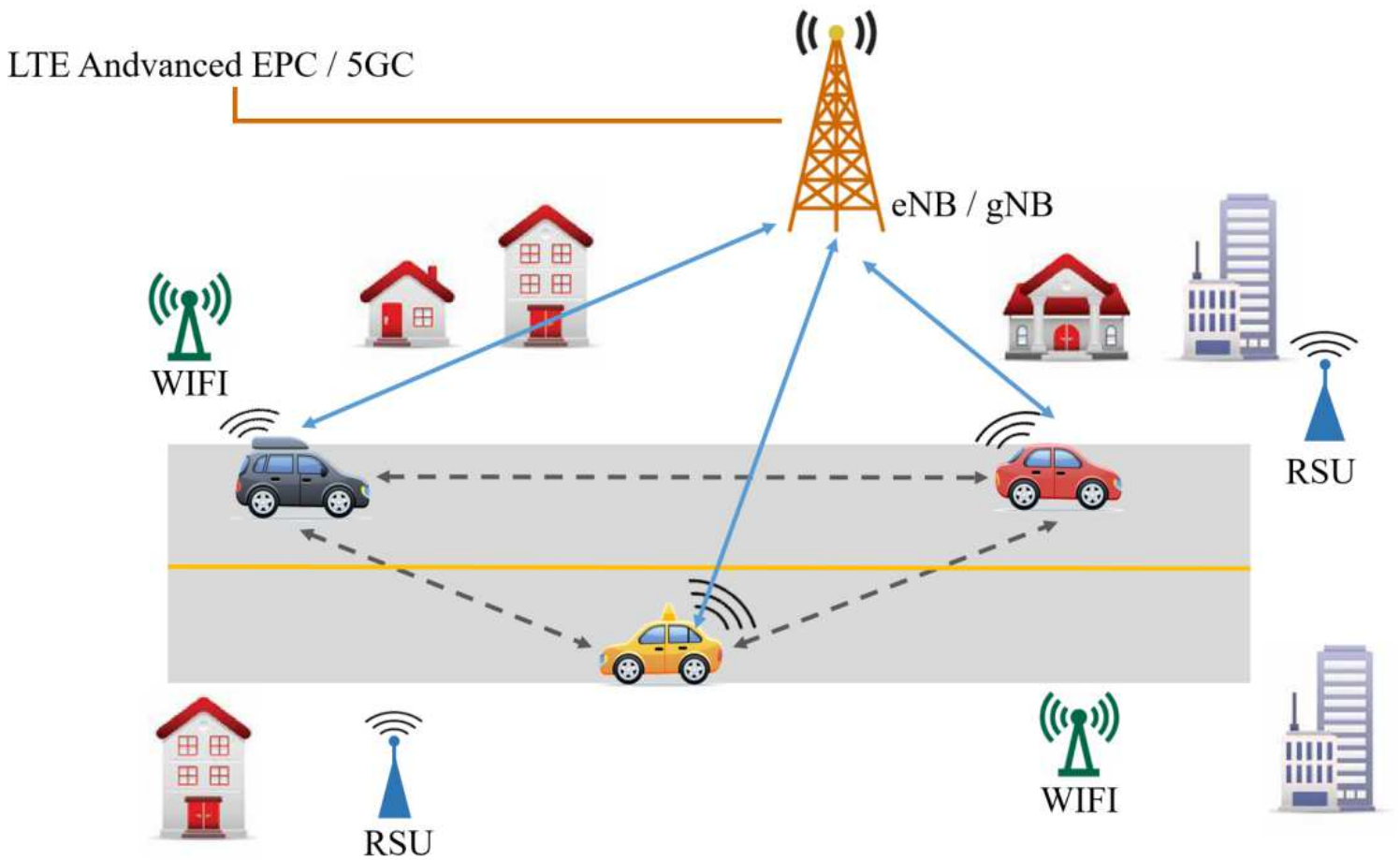


Figure 18

Internet of vehicles schematic diagram.

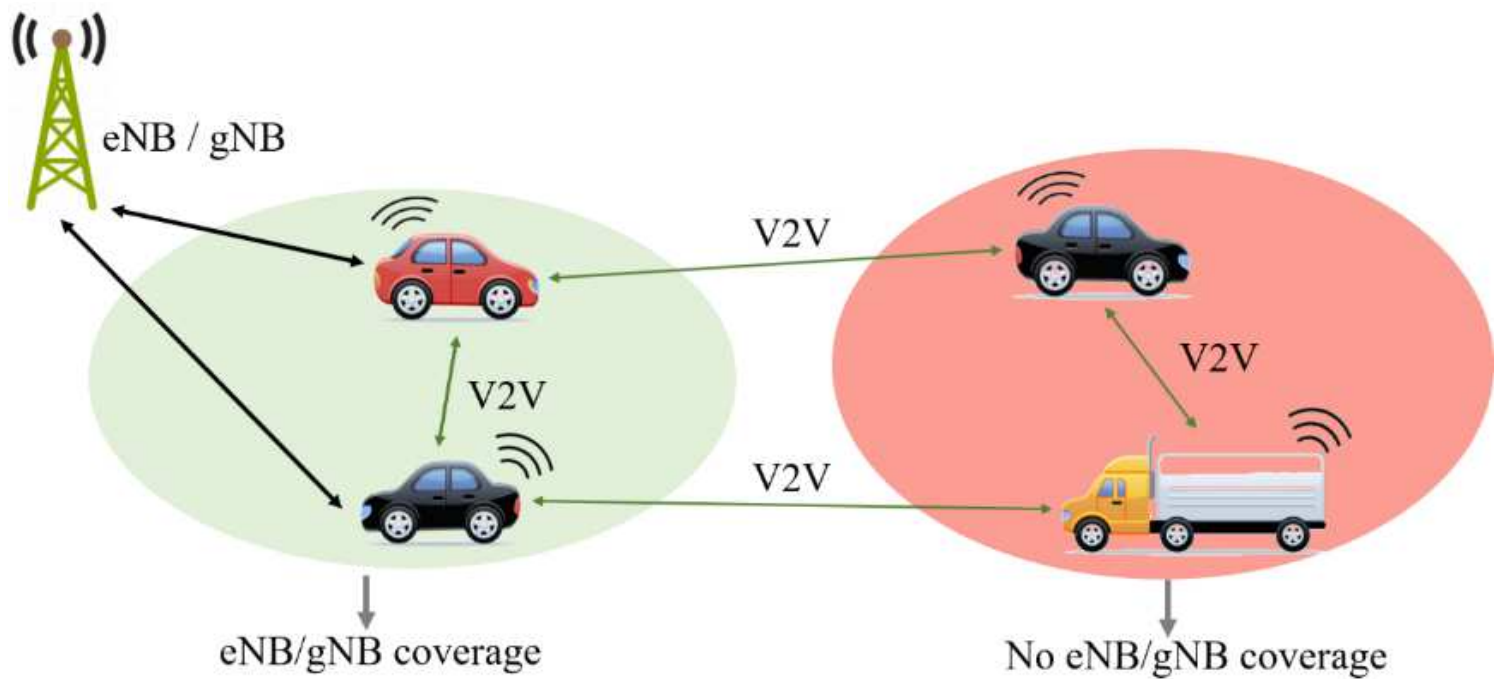


Figure 19

Vehicle antenna as micro node.

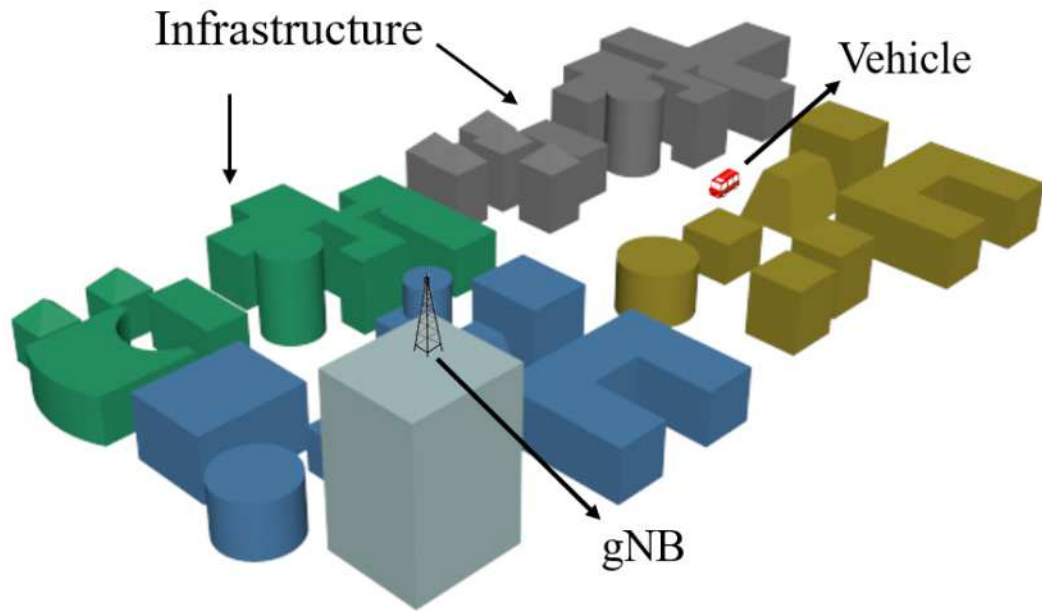


Figure 20

The three-dimensional view of simulating gNB of single sector coverage in urban.

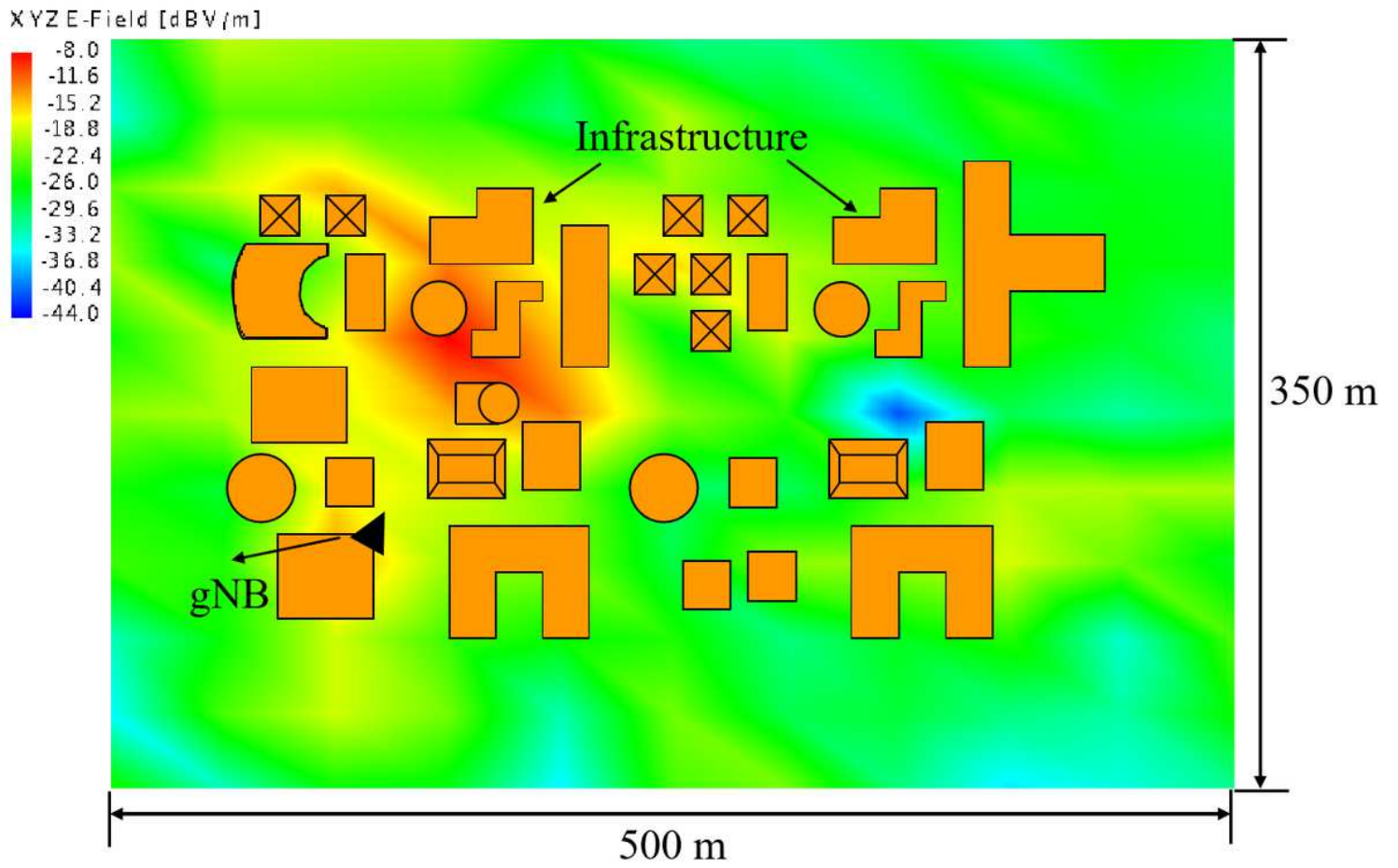


Figure 21

Distribution map of gNB of single sector coverage in urban environment.

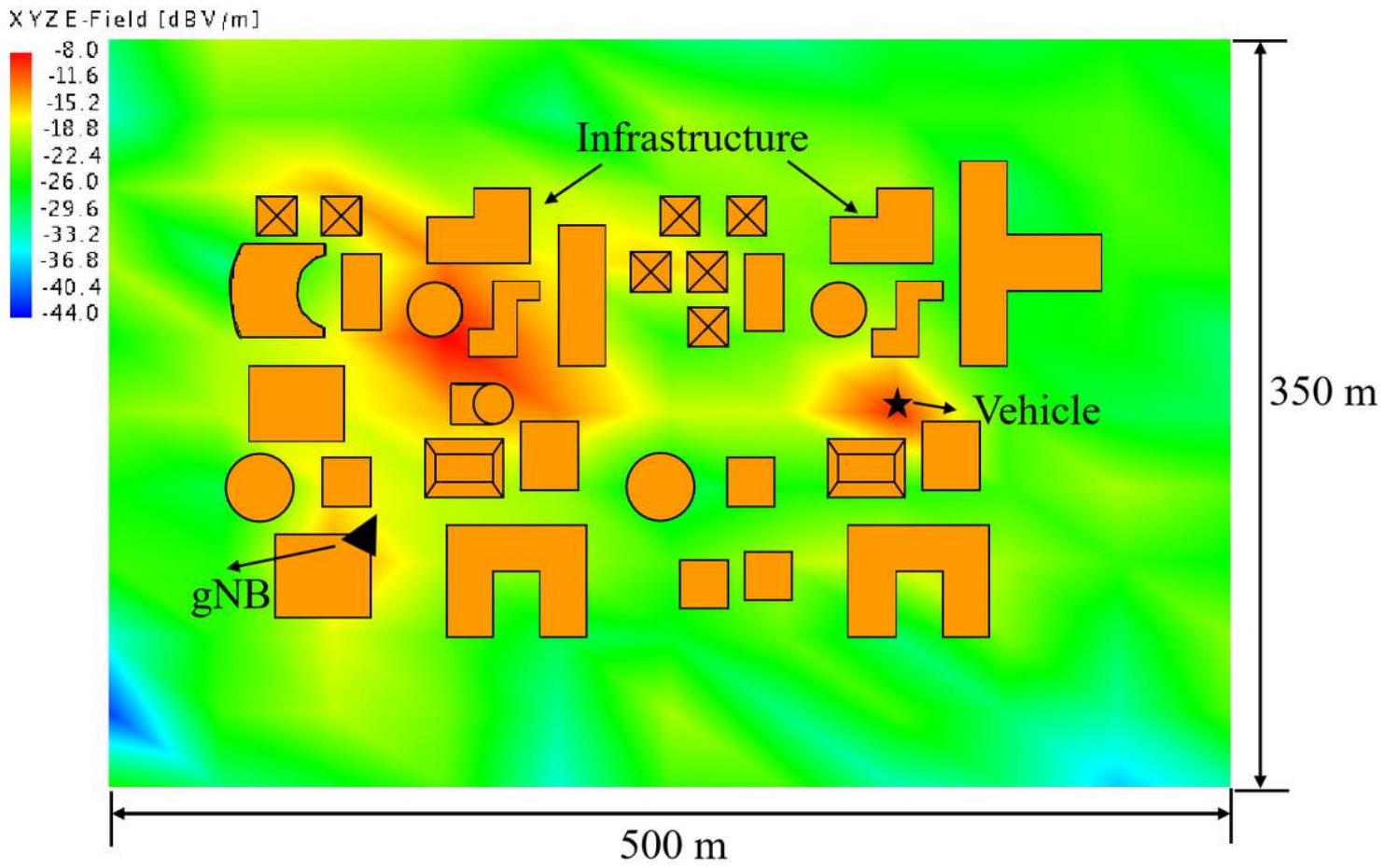


Figure 22

Supplementary effect drawing of blind area of mobile station for vehicle communication.